

Copyright  
by  
Joshua Paul White  
2009

**The role of Bud23 in the biogenesis of the small ribosomal subunit in  
*Saccharomyces cerevisiae*.**

**by**

**Joshua Paul White, BS.**

**Thesis**

Presented to the Faculty of the Graduate School of

The University of Texas at Austin

in Partial Fulfillment

of the Requirements

for the Degree of

**Master of Arts**

**The University of Texas at Austin**

**August 2009**

**The role of Bud23 in the biogenesis of the small ribosomal subunit in  
*Saccharomyces cerevisiae*.**

**Approved by  
Supervising Committee:**

---

---

## **Dedication**

I would like to dedicate this thesis to everyone who has supported me through this journey. Most of all I would like to dedicate this thesis to my family, who put up with my contrary nature that led me to a love of science and discovery, and my wife and best friend Amanda Kitchen, who has been there for me and sacrificed with me so that I could have an opportunity learn how to do the science that I love.

## **Acknowledgements**

I would like to thank and acknowledge all of my colleagues who have been invaluable during my time at the University of Texas at Austin. I would like to thank Arlen Johnson for giving me the opportunity to study ribosome biogenesis in his laboratory and for having the patience of a saint with his efforts to guide my professional growth. I would like to thank my fellow students and the post-doctoral fellows in Dr. Johnson's lab: Cyril Bussiere, Kai-Yin Lo, Nai-Jung (Ivy) Hung, Richa Sardana, Simrit Dhaliwal, and Peggy Huang. You were all there when I needed a question answered, something looked at, or a friend to talk to. I would also like to thank Dr. Scott Stevens and his lab: Yen-I "Grace" Chen, David "Josh" Combs, Leodis "Champ" Gupton, Rea Lardelli, Andrew "Adam" Roth, Jennifer Hennigan, and Matthew Sorenson. During our shared lab meetings and outside, I enjoyed the comments and criticism on my work, and the conversations. I would also like to thank Scott Stevens for reading and commenting on this thesis.

August 2009

## **Abstract**

### **The role of Bud23 in the biogenesis of the small ribosomal subunit in *Saccharomyces cerevisiae*.**

Joshua Paul White, MA

The University of Texas at Austin, 2009

Supervisor: Arlen Johnson

Ribosomes are the cellular structures responsible for the synthesis of protein in all branches of life. All ribosomes are made from a large and small subunit that in turn are composed of protein and RNA. The synthesis of eukaryotic ribosomes is a complex process involving more than 200 factors and spans three cellular compartments: the nucleolus, the nucleoplasm, and the cytoplasm. The precise function of most of these ribosome biogenesis factors remains unknown. The RNA component of ribosomes is in part processed from a large RNA transcript that yields most of the RNA present in mature ribosomes. Part of the maturation process involves modification of this ribosomal RNA as processing is carried out.

Recent work constructing protein interaction networks in *Saccharomyces cerevisiae* suggested the methyltransferase Bud23 was involved in ribosome biogenesis

[1]. This thesis describes my work to characterize Bud23 and place it within the ribosome biogenesis pathway. Bud23 is a SAM methyltransferase important for the proper biogenesis of the small ribosomal subunit. Here I will demonstrate that Bud23 methylates G1575 of the small subunit ribosomal RNA (SSU rRNA), and its absence delays export of the SSU rRNA from the nucleolus, and the nucleus, and results in the delayed maturation of the SSU rRNA. Finally, I will show that Bud23 function is connected to small subunit processome factor Utp14 through identification of a Utp14 mutant that suppresses the *bud23* $\Delta$  deletion phenotype.

## Table of Contents

List of Tables .....	vii
List of Figures .....	ix
List of Illustrations .....	x
Chapter 1 Introduction.....	1
1.1 Overview .....	1
1.2 Ribosome Biogenesis.....	3
1.2 Modifications of ribosomal RNA .....	5
1.4 Bud23.....	7
Chapter 2 Materials and Methods for Chapter 4.....	9
2.2 L- <sup>3</sup> H-[ <i>methyl</i> ]methionine Pulse Chase Labeling of rRNA .....	12
2.3 Fluorescent In-Situ Hybridization (FISH) .....	13
2.4 Cleavage of rRNA at m7G by Sodium Borohydride and Analine .....	14
2.5 Primer Extension of 18S rRNA.....	15
2.6 Sequence analysis of <i>BUD23</i> .....	16
Chapter 3 Materials and Methods for Chapter 5.....	17
3.1 Strains, plasmids, and oligonucleotides used in chapter 5.....	17
3.2 UV mutagenesis of <i>bud23Δ</i> .....	21
3.3 Testing for dominance/recessiveness of <i>bud23Δ</i> growth suppressor mutants.....	21
3.4 Polysome analysis using sucrose gradient fractionation.....	21
3.5.1 Gel and blotting.....	23
3.5 Hybridization .....	23
3.6 Genetic test for detection of aneuploidy .....	25
3.7 Construction of yeast genomic DNA library .....	25
3.7.1 Partial digest and purification of genomic DNA .....	25
3.7.2 Ligation into vector and purification of the library.....	25

3.8 Screening of AJY2683 DNA library for genes that improve the <i>bud23Δ</i> growth phenotype .....	28
3.9 Sequence analysis of <i>UTP14</i> .....	28
3.10 Structural prediction of the protein secondary structure around A758.....	28
Chapter 4 Results of characterization of Bud23 and phenotypes associated with <i>bud23Δ</i> strains .....	30
4.1 Introduction: Background work .....	30
4.2 Fluorescent in-situ hybridization of ITS1 confirms nuclear accumulation of pre-40S ribosomal subunits.....	36
4.3 L- <sup>3</sup> H-[ <i>methyl</i> ]methionine pulse chase labeling demonstrates defects in 18S formation .....	39
4.4.1 Justification for analyzing methylation of m7G1575 in <i>bud23Δ</i> cells.....	41
4.4.2 Primer extension analysis reveals that 18S rRNA G1575 is not methylated in a <i>bud23Δ</i> strain.....	44
4.4.3 m7G1575 cleavage supports primer extension data that Bud23 is necessary for methylation at G1575 .....	46
4.5 Discussion .....	50
Chapter 5 Identification and characterization of dominant suppressors of <i>bud23Δ</i> .....	58
5.1 Background .....	58
5.2 Testing for dominance/recessiveness of suppressor strains.....	63
5.3 Testing for aneuploidy in <i>bud23Δ</i> suppressor strains.....	63
5.4 <i>bud23Δ</i> suppressor comparison with multicopy RPS2 expression .....	69
5.5 Analysis of polysome profiles of <i>bud23Δ</i> suppressor mutant containing strains .....	71
5.6 Identification of Utp14 as the <i>bud23Δ</i> suppressor.....	73
5.5 Sequence comparison of Utp14.....	76
5.8 Secondary structure prediction of the region surrounding A758 .....	78
5.9 Discussion .....	81
Bibliography .....	89
Vita .....	93

## **List of Tables**

Table 2.1:	Strains used in Chapter 4.....	10
Table 2.2:	Plasmids used in Chapter 4 .....	10
Table 2.3:	Oligonucleotides used in Chapter 4 .....	11
Table 3.1:	Strains used in chapter 5.....	19
Table 3.2:	Plasmids used in chapter 5 .....	19
Table 3.3:	Oligonucleotides used in chapter 5 .....	20

## List of Figures

Figure 4.1: Polysomal and subunit analysis of WT and <i>bud23Δ</i> strains .....	32
Figure 4.2: 35S rRNA diagram with a detail of the ITS1 region showing northern blot probe sites.....	33
Figure 4.3: Northern blotting of rRNA processing intermediates in WT and <i>bud23Δ</i> cells .....	34
Figure 4.4: Localization of an Rps2-GFP reporter in WT and <i>bud23Δ</i> cells .....	35
Figure 4.5: Comparison of localization of ITS1 in WT and <i>bud23Δ</i> cells.....	38
Figure 4.6: Pulse chase analysis of rRNA processing in WT and <i>bud23Δ</i> cells	40
Figure 4.7: Sequence alignment of selected Bud23 (Ycr047c) homologs from different organisms .....	42
Figure 4.8: Primer extension of small subunit rRNA reveals lack of methylation at G1575 in a <i>bud23Δ</i> strain .....	45
Figure 4.9: Primer extension of small ribosomal rRNA following sodium borohydride/aniline cleavage confirms that <i>bud23Δ</i> strains lack m7G1575 .....	48
Figure 4.10: expression of methyltransferase deficient bud23 recovers growth of <i>bud23Δ</i> to nearly WT levels.....	49
Figure 4.11: Suppression of the <i>bud23Δ</i> growth phenotype by over expression of Rps2 .....	57
Figure 5.1: Mutants that suppress the <i>bud23Δ</i> phenotype .....	60
Figure 5.2: Confirmation of identity of <i>bud23Δ</i> suppressor strain by PCR .....	62

Figure 5.3: Southern blot demonstrating that the ratios of <i>RPS2</i> signal to <i>NMD3</i> signal are the same in WT, <i>bud23Δ</i> , and suppressor mutants.....	65
Figure 5.4: Comparison between <i>bud23Δ</i> suppressor AJY2683 and Rps2 multicopy suppression of the <i>BUD23</i> deletion phenotype .....	70
Figure 5.5: Polysomal profiles of WT, <i>bud23Δ</i> , suppressed <i>bud23Δ</i> , and isolated suppressor mutation indicate that suppression may be due to increased production of 40S subunits.....	72
Figure 5.6: Comparison suppression by <i>RPS2</i> and Utp14(A758G) .....	75
Figure 5.7: PSI-Blast of the region surrounding Utp14 A758 .....	77

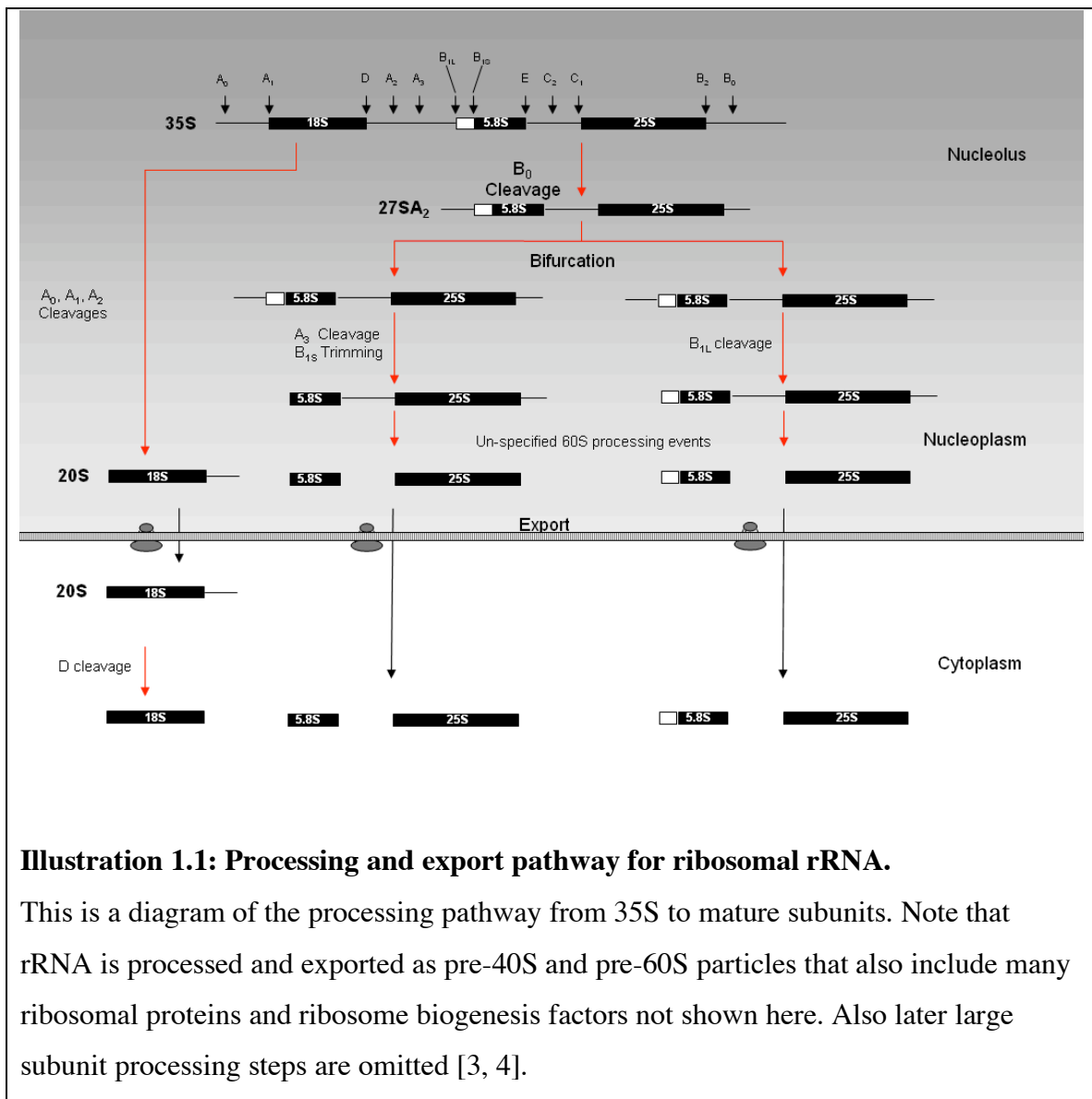
## List of Illustrations

Illustration 1.1: Processing and export pathway for ribosomal rRNA .....	2
Illustration 4.1: Diagram of a CG base pair .....	53
Illustration 5.1: Tetrad analysis of dominant mutant cross with a <i>trp1Δ</i> strain ...	67
Illustration 5.2: Tetrad analysis of aneuploid phenotype cross with a <i>trp1Δ</i> strain .....	68
Illustration 5.3: Diagram of the insert identified from the AJY2683 genomic library .....	74
Illustration 5.4: GeneSilico secondary structural prediction of Utp14 .....	80
Illustration 5.5: for the role of Utp14 and Bud23 in 40S biogenesis .....	87

## Chapter 1: Introduction

### 1.1 Overview

As every cellular system carries out the multitude of functions needed for growth and continued survival, there are some constants that all life forms seem to share. One of these constants is the RNA mediated transformation of genetic information into proteins by ribosomes. Ribosomes are one of the largest and most complicated molecular structures synthesized in living cells. For the study of ribosome biogenesis in eukaryotes, brewers yeast (*Saccharomyces cerevisiae*) has been very useful. *S. cerevisiae* ribosomes consist of four ribosomal RNA molecules (rRNA) and more than eighty proteins that form the mature 40S and 60S ribosomal subunits. The small subunit contains the 18S rRNA and 32 ribosomal proteins and the large subunit contains the 25S, 5S and 5.8S rRNA and 46 ribosomal proteins [2]. Of this complement of 68 ribosomal proteins, 59 exist as pairs of paralogs. The biogenesis of these subunits is a very complex process that requires more than 200 accessory proteins and spans three cellular compartments [3, 4] (Illustration 1.1).



## 1.2 Ribosome Biogenesis

Ribosome biogenesis begins in the nucleolus where a large 35S precursor RNA is synthesized by RNA polymerase I. This RNA then associates with biogenesis factors and ribosomal proteins, mostly specific for the small subunit (SSU). After these factors and proteins bind to the 35S, the RNA collapses into a structure that has been named the SSU processome, or 90S particle [5-7]. This structure has been visualized by transmission electron microscopy as small terminal knobs on the ends of 35S transcripts [8]. The role of the small subunit processome is to create a pre-40S particle and prepare the remaining rRNA for production of the 60S. Pre-40S processing events include: cleavage at site A0, A1 in the 5' end of the 35S precursor binding of SSU proteins, and a collection of biogenesis factors. Cleavage at site A2 by an unidentified endonuclease releases 20S rRNA which eventually forms the mature 18S rRNA. The remainder of the 35S then continues on to form the 60S (below). After the A2 cleavage the pre-40S then travels from the nucleolus, through the nucleoplasm, and is exported from the nucleus in a manner dependant on the karyopherin Crm1 and the Ran-GTPase cycle [9]. In the cytoplasm, the 40S subunit is matured in a process involving a dimethylation of the 3' end of the 18S by Dim1, and a cleavage event at site D that converts 20S rRNA into 18S, possibly carried out by Nob1 [3, 10]. Mutants of proteins involved in 40S biogenesis can show a nucleolar, [11] nuclear [12, 13], or cytoplasmic [14] localization of small subunit proteins and RNA depending on what step in biogenesis they play a role.

The 60S large subunit (LSU) follows a more complicated biogenesis pathway. After the A2 cleavage event, large subunit proteins and large subunit biogenesis factors

associate with the remainder of the 35S rRNA, the 27SA2 rRNA. At this point the LSU can be formed by one of two pathways that produce slightly different forms of 5.8S that differ by a small number of nucleotides, but leaves the 25S unaltered [3, 4]. The significance of these different forms of 5.8S remains unknown. The 5S rRNA of the LSU is transcribed by RNA polymerase III independently of the 35S. After further maturation the pre-60S is then exported from the nucleus in a Crm1-dependent manner [3, 4] to the cytoplasm where its biogenesis is completed.

Ribosome biogenesis factors include: helicases, nucleases, ATPases, GTPases, methyltransferases, chaperones, various isomerases, snoRNPs, and other factors whose functions remain largely unknown [3]. Functional prokaryotic ribosomes can be assembled in vitro with only  $\text{MgCl}_2$ , ribosomal proteins, ribosomal RNAs, and a few brief heating steps [15]. The general outline of the assembly map has been worked out in prokaryotes, demonstrating the order of binding of the various ribosomal proteins and the general major steps in assembly [16]. Recent evidence indicates that assembly of the *S. cerevisiae* 40S may be very similar to its prokaryotic counterparts [17], however functional yeast ribosomes have never been assembled in vitro. The heat-induced self-assembly implies that some biogenesis factors may be chaperones and largely guide a self-assembly process and perhaps prevent inappropriate folding and other dead-end interactions during biogenesis, especially in more complicated eukaryotic systems. Connected to this is the idea of “quality control” aspects of ribosome biogenesis factor function. Quality control has been discussed in several studies [3, 18, 19] and examples of malformed or unformed particles have been observed which may represent failures of

a quality control mechanism [18, 20]. “Structural proofreading” [12, 21, 22] is a similar concept that has been used with respect to proteins that modify rRNA. Briefly, structural proofreading argues that the successful binding of some ribosome biogenesis factors signals a completed stage of maturation.

### **1.3 Modifications of ribosomal RNA**

During ribosome biogenesis the rRNAs of both subunits are modified in a large variety of ways aside from the cleavage events. These modifications include: isomerizations of uridine to pseudouridine, methylation of the rRNA ribose at the 2' hydroxyl, and especially in eukaryotes a large number of specific base modifications [3, 4, 23]. The pseudouridine and 2'-O-methylations make up most of the modifications and are carried out by two general systems that use specific guide snoRNAs for positional specificity [3, 4, 24]. The base modifications are diverse and are usually carried out by specific proteins that modify specific bases ([3, 4, 12, 19, 23]. The purpose of these modifications is still mysterious. Most modifications are highly conserved between closely related species, but with only one exception are not universally conserved among all organisms [3, 19]. The fact that most of these modifications seem to be clustered around functionally important centers argues for their importance [23]. But mutations that prevent even several modification at a time seem to have little effect [25-27]. In fact no single modification has been found that is essential; however, there are several hypotheses that try to explain their presence in ribosomes.

One possible explanation is that the proteins responsible for the modifications are more important than the modifications themselves. One example is the methyltransferase KsgA [28]. KsgA is the *E. coli* homolog of the *S. cerevisiae* protein Dim1 [29]. This protein is responsible for the universally conserved adenine dimethylation at the 3' end of the 18S. While essential in yeast, deletion of *KSGA* in *E. coli* only causes a moderate growth phenotype and decreased translational fidelity [19]. Despite being essential, expression methyltransferase deficient forms of Dim1 grew comparably to wild type strains [19]. A similar story exists for another small subunit biogenesis factor, Emg1[30]. Thus it seems possible that many proteins that modify rRNA are primarily important for recognition and/or creation of specific, correctly formed precursor particles and secondarily important for the modifications they catalyze.

The second explanation for the presence of the modifications is that each modification provides minor alterations to the structure of the ribosome that allow for efficient ribosomal maturation and/or translation within the context of the whole ribosome. Individually, preventing the modifications show little or no effect. Effects only become more severe when multiple modifications are prevented. *T. aquaticus* ribosomes reconstituted in vitro without modifications show mild in vitro translational effects [26]. Recent in vivo work in yeast combined up to six deletions of genes encoding snoRNAs that guide pseudouridine modifications in the peptidyl transferase center [27]. Mild growth phenotypes and polysome profiles problems were reported, but only for a single, unique site among the six tested, or the other five combined. Combining the six mutants resulted in a strain that grew only slightly worse than the unique site. Another recent

work in yeast tested strains deleted for guide snoRNA genes under a wide variety of growth conditions [25]. These snoRNAs specifically guided the methylation of 2' hydroxyl modifications. The result was that the lack of specific methylations had different effects on the growth of the various deletion strains. Some grew better than wild type (*snr67Δ* in DTT) while others grew worse (*snr52Δ* caffeine). More recent work by the Fournier group demonstrates similar results in an intersubunit bridge [31], and in the decoding center [32]. An analysis of rRNA modifications from a different perspective moved locations of modifications to important regions of the peptidyl transferase center by changing the sequences of their associated snoRNAs [33].

Considering the evidence presented in many studies, the following picture seems likely. The associated modifying enzymes play important roles in biogenesis outside of modification. For the modifications themselves it seems that they have small roles in overall structure and function that are usually only detectable in aggregate. A workable analogy would be the mechanism inside a watch. If a few teeth are missing an effect might not be noticed. If many teeth are missing or put in the wrong place the effects become much stronger and start to observably impact proper function. These modifications may have influences only under specific conditions, or while translating specific classes of mRNA or while engaging in specific forms of translational regulation such as frame shifting. One modification may tweak translation one way when it is colder, another may alter translation when conditions are more or less saline. What seems dispensable in the lab may in fact provide a growth advantage when one considers the challenges faced by a single yeast on a grape in nature.

## 1.4 Bud23

A mutant of Bud23 was originally identified as a mutant in bud site selection [34]. Normally, ellipsoid diploid yeast cells bud at one of either of the two poles, and haploid yeast cells bud at the same pole from which they had previously budded from. Bud site selection mutants display aberrations from this pattern. Specifically, the *bud23Δ* strain was identified as a slow-growing strain that reproduced in a randomly budding pattern. A potential role for Bud23 in small subunit biogenesis was hinted at in recent work involving pre-40S tandem affinity purifications (TAP) which allow sequential purification of protein complexes using two tags [7]. Work to validate methods of generating protein interactions maps also indicated that Bud23 may be involved in ribosome biogenesis [1]. A *bud23Δ* mutant was shown to have a polysome profile and steady state rRNA levels that indicate a problem with small subunit biogenesis (Figures 1-4) [12]. Specifically there was an increase in the 20S:18S ratio and a nuclear accumulation of an Rps2-GFP reporter. Analysis of primary amino acid sequence of Bud23 indicated that it likely functions as an *S*-adenosylmethionine-dependent methyltransferase (figure 7). At the time this analysis of the *bud23Δ* strain was carried out one modified base of the yeast 18S rRNA had no associated methyltransferase, the 7-methylguanine at G1575 (m7G1575) [35]. Taken together these data strongly indicated that exploration of a link between Bud23 and m7G1575 was worth pursuing. In this thesis I present my work demonstrating the Bud23 is responsible for methylation of G1575. Also in work directed at understanding the function of Bud23 I present the results of a

screen for suppressors of *bud23Δ* that revealed the small subunit processome component Utp14.

## **Chapter 2: Materials and Methods for Chapter 4**

This section contains all materials and methods for experiments performed in chapter four. When an experiment is first mentioned it will be fully described. Subsequent mentions will refer to the first exposition and include any necessary deviations.

### **2.1 Strains, Plasmids, and Culturing Media used in Chapter 4**

Tables 1-3 list all strains used in chapter 4. Transformations and other genetics methods were all carried out as previously described [36]. The *bud23Δ* strain AJY2161 was isolated from the heterozygous diploid deletion collection [37]. All wild type comparisons were made with BY4741 (AJY1942) unless otherwise noted. Unless otherwise indicated all strains were grown in YPD (rich medium) or synthetic dropout media at 30°C with 2% glucose for liquid media, and with 2% agar plates for solid media.

Table 2.1: Strains used in Chapter 4			
Strain	Alias	Genotype	Reference
AJY1539	N/A	MATa <i>his3Δ leu2Δ ura3Δ CRM1T539C</i>	Hedges et al
AJY1942	BY4741	MATa <i>his3Δ leu2Δ met15Δ ura3Δ</i>	Brachmann et al 1998
AJY2161	N/A	MATa <i>bud23Δ::KanMX his3Δ leu2Δ ura3Δ lys2Δ met15Δ</i>	White et al 2008

Table 2.2: Plasmids used in Chapter 4			
Plasmid	Alias	Genotype	Reference
pAJ99	pRS415	<i>CEN LEU2</i>	Christianson et al 1992
pAJ726	N/A	2u <i>LEU2</i> 35S rDNA locus	A. Johnson unpublished
pAJ1629	N/A	<i>CEN MET15 SIK1-mRFP</i>	White et al 2008
pAJ2051	pRS411	<i>CEN MET15</i>	Cost et al 1996
pAJ2154	N/A	<i>CEN LEU2 BUD23</i>	White et al 2008
pAJ2155	N/A	<i>CEN LEU2 bud23(D77K)</i>	White et al 2008
pAJ2156	N/A	<i>CEN LEU2 bud23(G57E)</i>	White et al 2008
pAJ2151	N/A	<i>CEN LEU2 BUD23-GFP</i>	White et al 2008
pAJ2163	N/A	<i>CEN LEU2 BUD23-13xMYC</i>	This work

<b>Table 2.3: Oligonucleotides used in Chapter 4</b>	
Oligonucleotide	Sequence
AJO1024	ATGCTCTTGCCAAAACAAAAAATCC ATTTTCAAATTATTAAATTTCTT
AJO1027	TGTGTACAAAGGGCAGGGACGTA

## 2.2 L-<sup>3</sup>H-[*methyl*]methionine Pulse Chase Labeling of rRNA

Cells were transformed with the *MET15* containing vector pAJ2051 and grown in 20ml of met- dropout media to an OD<sub>600</sub> of ~0.2. Cells were then collected and resuspended in 3ml of met<sup>-</sup> medium pre-warmed to 30°C, and incubated at 30°C for 25 minutes. Cells were then labeled with 0.3 mCi L-<sup>3</sup>H-[*methyl*]methionine for two minutes. Unlabeled methionine was then added to a final concentration of 0.6 mM and samples were taken over 15 minutes. Each sample was centrifuged for 8 seconds, the supernatant quickly removed, and the tube containing the pellet flash frozen in liquid nitrogen. RNA was then extracted from all samples using an Epicentre Biotechnologies “Masterpure Yeast RNA Purification Kit”, resuspended in 1x TE buffer and stored at -80°C. Next, 5.75 µg of total RNA was then electrophoresed through a 1.2% formaldehyde 1x MOPS (3-[N-Morpholino]propanesulfonic acid) gel, and transferred to a nylon membrane. This membrane was then sprayed with Dupont En<sup>3</sup>hance according to manufacturer’s instructions and exposed to film for six days at -80°C.

### **2.3 Fluorescent In-Situ Hybridization (FISH)**

Cells were grown to an OD<sub>600</sub> of ~0.3 and then prepared for FISH using a protocol adapted from <http://singerlab.aecom.yu.edu/protocols/>. Cells were fixed for 30 minutes at room temperature in flasks while agitating by adding formaldehyde and glacial acetic acid to 4.5% and 11% respectively. Next cells were washed twice with 0.1 M potassium phosphate buffer (pH 7.5) and once with 0.1 M potassium phosphate (pH 7.5) and 1.2 M sorbitol. Cells were then spheroplasted in the same phosphate/sorbitol buffer in the presence of 20 mM vanadyl-Ribonuclease complex (Sigma), 28 mM  $\beta$ -mercaptoethanol, 0.06 mg/ml PMSF, and 50 mg/ml Zymolyase T-20 for 10 min at 37°C. Cells were then adhered to poly-lysine coated slides and placed in 70% ethanol at -20°C for no longer than a two weeks. After rehydration with 4x SSC (0.6 M sodium chloride, 0.06 M sodium citrate) cells were prehybridized in 50% formamide, 10% dextran sulfate, 4x SSC, 1x Denhardt's solution, 20 mM vanadyl-RNase complex for one hour at 37°C. Next the prehybridization buffer was replaced with the same buffer containing 1 ng/ $\mu$ l Cy3-labeled AJO1024 and hybridized for 20 hours at 37°C in a humid chamber. Cells were then washed once with 2x SSC, once with 1x SSC, and once with 1x PBS (phosphate buffered saline). DNA was then stained with 4',6'-diamidino-2-phenylindole (DAPI) in 1x PBS. Cells were washed once more in 1x PBS and mounted in Aqua Poly/Mount (Polysciences Inc). Cells were then observed for fluorescence using a Nikon E800 microscope fitted with a 100X objective and a Photometrics CoolSNAP ES digital camera controlled with NIS-Elements AR 2.10.

## **2.4 Cleavage of rRNA at m7G by Sodium Borohydride and Analine**

This method of m7G cleavage is based on the methods outlined in [38]. Unless otherwise noted all reagents were kept on ice during the procedure. Cells were grown to an  $A_{600}$  of ~0.3 and total RNA was isolated from cells with a Masterpure Yeast RNA extraction kit. Next, 1  $\mu$ g of total RNA in 1  $\mu$ l was added to 20  $\mu$ l 0.5 M Tris-HCl pH 8.2, 0.5 M sodium borohydride (from a freshly made stock), and 20  $\mu$ g methylated carrier RNA (see below). This was then incubated for 5 minutes at 20°C in total darkness. Next 200  $\mu$ l of 0.6 M sodium acetate at pH 5.5 was added with 3 volumes of 100% ethanol to precipitate RNA. RNA was then immediately centrifuged, washed with 80% ethanol, air dried and resuspended in 80  $\mu$ l of water. 20  $\mu$ l of 1:3 analine:acetic acid was then added and incubation was carried out in total darkness for two hours at room temperature. Next, 200  $\mu$ l of 0.3 M sodium acetate and 900  $\mu$ l 100% ethanol was added to precipitate RNA. The sample was then immediately pelleted by centrifugation, washed with 100% ethanol, air dried and resuspend in 10  $\mu$ l of water. This sample was used as input for a primer extension reaction identically to below.

Methylated carrier RNA was synthesized as follows. 1 mg of purified yeast tRNA in 40  $\mu$ l of water was added to 300  $\mu$ l of 50 mM sodium cacodylate pH 5.5, 1 mM EDTA. 5  $\mu$ l of dimethylsulfate was then added to this solution and the solution was then mixed, incubated for five minutes at 90°C, and then chilled on ice. Next 75  $\mu$ l of 1 M tris-acetate pH 7.5, 1.5 M sodium acetate, 1 M  $\beta$ -mercaptoethanol, and 900  $\mu$ l of 100% ethanol was added. The solution was then mixed and flash frozen in liquid nitrogen and centrifuged at full speed for 8 minutes. The supernatant was then removed and the pellet resuspended in 375  $\mu$ l of 0.3 M sodium acetate and then 1.5 ml of 100% ethanol was added. The pellet

was then centrifuged again, the supernatant removed, and the pellet washed with 80% ethanol. The pellet was then air dried and resuspended in water to a concentration of 10 mg/ml and stored at -80°C.

## **2.5 Primer Extension of 18S rRNA**

Cells for m7G cleavage were transformed with indicated *LEU2* vectors according to standard methods [36]. Cells were then grown in leu<sup>-</sup> dropout media to an A<sub>600</sub> of 0.3. Primer extension only cells were grown in YPD to an A<sub>600</sub> of 0.3. Total RNA was then extracted with a Masterpure Yeast RNA extraction kit identically to the above pulse-chase work. The oligonucleotide used in primer extension and DNA sequencing lanes was AJO1027 end-labeled using 3 µl of 10 mCi/ml [ $\gamma$ -<sup>32</sup>P]ATP (PerkinElmer) in a reaction with 1 µl of 10 pmol/µl oligonucleotide and 10 units of T4 polynucleotide kinase (New England Biolabs). Products were purified using a Biogel P-20 (BioRad) size exclusion column by centrifugation. DNA sequencing ladders were made using a USB sequenase version 2.0 DNA sequencing kit and a plasmid containing a wild type 18S rDNA sequence (pAJ726). Primer extension using 12 µg of total RNA was carried out as described previously [39] except that denaturation was carried out in water. Labeled DNA obtained by the primer extension and DNA sequencing reactions were then separated on an 8% denaturing urea polyacrylamide gel. The gel was then dried and exposed a phosphor storage screen (Kodak) and scanned using a BioRad Molecular Imager FX scanner.

## 2.6 Sequence analysis of Bud23

Searches for *BUD23* homologs was carried using the National Center for Biotechnology Information “protein blast” [40] located at <http://blast.ncbi.nlm.nih.gov/Blast.cgi>.

Alignment of Bud23 homologs was carried out using a ClustalW2 sequence alignment program [41]. The alignment was constructed from sequences from the following organisms using the associated accession numbers: *Danio rerio* NP\_001076348, *Mus musculus* NP\_079651, *Candida glabrata* XP\_449239, *Xenopus laevis* AAH71142, *Gallus gallus* NP\_001034421, *Homo sapiens* NP\_059998, *Drosophila melanogaster* NP\_649762, *Caenorhabditis elegans* NP\_498051, *Arabidopsis thaliana* NP\_200538.

## Chapter 3: Materials and Methods for Chapter 5

### 3.1 Strains, plasmids, and oligonucleotides used in chapter 5

Tables 4-6 list all strains, plasmids, and oligonucleotides used in chapter 4. Transformations and other genetics methods were all carried out as previously described [36]. The *bud23Δ* strain AJY2161 was isolated from the heterozygous diploid deletion collection [37]. All wild type comparisons were made with BY4741 (AJY1942) unless otherwise noted. The clonate resistant *bud23Δ* strain AJY2676 was generated by digestion of p4339 with EcoRI, purification of the 1kb fragment, transformation of that fragment into AJY2161, and selection of clonate resistant colonies that grew at the same rate as AJY2161. The MAT $\alpha$  WT strain AJY2293 was isolated from a tetrad dissected from the heterozygous diploid deletion collection (*kap123Δ* strain). The spontaneous suppressor of the *bud23Δ* growth phenotype AJY2683 was isolated from AJY2676. The mutagenesis derived suppressor of the *bud23Δ* growth phenotype AJY2684 was made by UV mutagenesis of an exponentially growing culture of AJY2676. The MAT $\alpha$  version of AJY2683, AJY2685, was generated by mating AJY2683 to AJY2293, sporulating, and isolating a slow growing colony of appropriate mating type. The BY4741 *trp1Δ* strain, AJY2686, was a kind gift from Scott Stevens (strain SS4019). The strain carrying the suppressor mutant and wild type *BUD23* AJY2688 was isolated by mating AJY2683 with AJY2293 and selecting 2:2, *bud23Δ*:WT tetrads by growth rate and saving the WT size

colonies. Finally the *trp1* $\Delta$  *bud23* $\Delta$  strain was constructed by transforming AJY2686 with a PCR fragment derived from AJY2161 and primers AJO1034 and AJO1035. Slow growing colonies that grew on G418 were selected by growth comparison with known *BUD23* deletion strains. Unless otherwise indicated all strains were grown in YPD (rich medium) or synthetic dropout media at 30°C with 2% glucose, or 2% plates for solid media.

Table 3.1: Strains used in chapter 5			
Strain	Alias	Genotype	Reference
AJY1942	BY4741	MATa <i>his3Δ leu2Δ met15Δ ura3Δ</i>	Brachmann et al 1998
AJY2293	N/A	MATα <i>leu2Δ ura3Δ met15Δ his3Δ</i>	This work
AJY2676	N/A	MATa <i>bud23Δ::NatMX his3Δ leu2Δ ura3Δ lys2Δ met15Δ</i>	This work
AJY 2682	N/A	MATα <i>bud23Δ::KANMX his3Δ leu2Δ ura3Δ met15Δ</i>	This work
AJY2683	S1	MATa <i>bud23Δ::NatMX his3Δ leu2Δ ura3Δ lys2Δ met15Δ</i>	This work
AJY2684	UV8	MATa <i>bud23Δ::NatMX his3Δ leu2Δ ura3Δ lys2Δ met15Δ</i>	This work
AJY2685	N/A	MATα <i>bud23Δ::NatMX his3Δ leu2Δ ura3Δ lys2Δ met15Δ</i>	This work
AJY2686	SS4019	MATa <i>his3Δ leu2Δ met15Δ ura3Δ trp1Δ</i>	This work
AJY2687	N/A	MATa <i>bud23Δ::NatMX his3Δ leu2Δ met15Δ ura3Δ trp1Δ</i>	This work
AJY2688	S1 single	MATα <i>his3Δ leu2Δ met15Δ ura3Δ</i>	This work

Table 3.2: Plasmids used in chapter 5			
Plasmid	Alias	Genotype	Reference
pAJ57	pRS426	<i>2u URA3</i>	Sikorski et al 1989
pAJ100	pRS416	<i>CEN URA3</i>	Sikorski et al 1989
pAJ123	N/A	<i>CEN NMD3 LEU2</i>	Ho et al 1999
pAJ1037	p4339	Not a yeast vector, see reference	Tong et al 2001
pAJ1399	N/A	<i>CEN RPS2-eGFP HIS3</i>	White et al 2008
pAJ1652	N/A	<i>2u URA3 RPS2</i>	This work
pAJ1654	N/A	<i>2u URA3 BUD23</i>	This work
pAJ1918	N/A	<i>CEN URA3 UTP14(A758G)</i>	This work
pAJ1919	N/A	<i>CEN URA3 UTP14</i>	This work

Table 3.3: Oligonucleotides used in chapter 5	
Oligonucleotide	Sequence
AJO786	TCCGATTTCGTTCGTCCGATT
AJO1034	CGCTAAACGAGTCCAACC
AJO1035	CTTTTACTGATGAGCTTCC
AJO1293	CAACCAGGTAAAGTGGTATC
AJO1294	TTGGATTCCAAGGAACCTGG
AJO1295	CTCTCATCAATCTCATTTTCG
AJO1296	AGCGTCTTCGTCATCATTGC
M13F	GTTTTCCCAGTCACGAC
M13R	AGCGGATAACAATTCACACAGGA

### **3.2 UV mutagenesis of *bud23Δ*.**

AJY2676 was grown in 50 ml YPD liquid culture to an  $A_{600}$  of ~0.4. Cells were centrifuged in a Beckman JA-12 rotor at 3000RPM and washed with 20 ml double distilled sterile  $H_2O$  (dd $H_2O$ ). Cells were centrifuged again and resuspended in dd $H_2O$  to a concentration of  $3 \times 10^7$  cells/ml. Cells were then divided into four aliquots. One part was set aside as a negative UV control. The remaining parts were exposed to UV in a sterile medium weigh boat using 25,000, 50,000 or 100,000uJ of energy with a Stratagene UV Stratalinker 1800. The samples were then pelleted and resuspended in 16% glycerol and stored at  $-80^\circ C$ . The 25,000uJ sample with a ~10% survival rate was chosen for mutant screening and was plated out on YPD at ~5000 colonies per plate. Colonies growing faster than unmutagenized AJY2676 were picked, patched and stored in 16% glycerol at  $-80^\circ C$ .

### **3.3 Testing for dominance/recessiveness of *bud23Δ* growth suppressor mutants.**

AJY2676 mutants were mated with AJY2682 and diploids were selected on YPD/G418/Clonat. Single colonies were isolated and growth was compared to AJY2676xAJY2682. Dominant mutants displayed greater growth than AJY2676xAJY2682 and recessive mutants displayed growth equal to AJY2676xAJY2682.

### **3.4 Polysome analysis using sucrose gradient fractionation**

200 ml of cells were grown in YPD to an  $A_{600}$  of 0.3. Cyclohexamide was added to a final concentration of 150  $\mu\text{g/ml}$  and then cells were immediately harvested by pouring into centrifuge bottles over ice. Cells were centrifuged for 5 minutes at 5,000 RPM in a Beckman JLA-10.5 rotor. Cells were then resuspended in a small volume of the remaining buffer, re-pelleted in 50 ml conical vials and cell pellets were stored at  $-80^{\circ}\text{C}$ . Cells were then thawed and washed once in lysis buffer (10 mM Tris-HCl pH 7.5, 10 mM magnesium chloride, 6 mM  $\beta$ -mercaptoethanol, 100 mM potassium chloride, 150  $\mu\text{g/ml}$  cyclohexamide, 1 mM phenylmethylsulphonyl fluoride, 1  $\mu\text{M}$  leupeptin, and 1  $\mu\text{M}$  pepstatin-A). Cells were then resuspended in an equal volume of lysis buffer, and then an equal volume of ice cold glass beads were added (equal to cells+buffer). Cell membranes were then sheared by vortexing six times using a VWR vortex-genie 2 set to number six with one minute on ice between each vortex. Lysed cells were then centrifuged in a TOMY MTX-150 desktop refrigerated centrifuge at full speed for ten minutes at  $4^{\circ}\text{C}$ . The supernatant was then removed to a pre-chilled new tube and identically re-centrifuged. The supernatants were then standardized to the sample with the lowest concentration using at  $A_{260}$  absorbance reading with more lysis buffer. Nine  $A_{260}$  units of extract were then layered onto a 7-47% sucrose gradient and centrifuged at 37,000 RPM for 2.5 hours using a Beckman SW40 rotor. These gradients were then fractionated using an ISCO model 640 density gradient fractionator with an attached absorbance monitor set to 254 nm.

### **3.5 Southern blots**

#### **3.5.1 Gel and blotting**

Strains to be tested were grown in YPD to saturation and DNA extracted according to standard Zymolyase preparations [36]. 4 µg of DNA from selected strains were digested with EcoRI, separated on a 0.8% agarose gel in 1x TAE containing ethidium bromide. HindIII cut lambda phage genome ladder that was end labeled with  $\alpha$ -<sup>32</sup>P dCTP (PerkinElmer) by klenow (New England Biolabs) was used as a molecular weight marker. Next the gel was imaged under UV fluorescence on a UVP Biodoc-It transilluminator. The DNA was then depurinated in 0.25 M HCl for 30 min, denatured in 0.5 N sodium hydroxide for 30 min, and neutralized in 0.5 M Tris-HCl, pH 7.4, 3 M sodium chloride for 30 min. Next the gel was soaked in 20x SSC for 30 min, and then the DNA was then transferred to Bio-Rad Zeta-Probe GT nylon membrane by downward capillary transfer (Schleicher & Schuell Turboblotter transfer system). After overnight transfer the membrane was washed once gently with 2x SSC and cross-linked using a Stratagene UV Stratalinker 1800 using auto crosslink settings. The gel was also re-imaged to confirm efficient transfer.

#### **3.5.2 Hybridization**

The above membrane was pre-hybridized while rotating in 10 ml 0.25 M sodium phosphate pH 7.2, 7% SDS, and 1 mM EDTA in a Bellco short screw cap glass bottle

using a Bellco Autoblot micro hybridization oven set to 65°C. Pre-hybridization buffer was replaced by 10 ml of the same buffer and  $1.5\text{-}2 \times 10^6$  CPM heat denatured probe (~10  $\mu\text{l}$ ) was added. The *NMD3* probe was an ~850bp fragment cut from pAJ123 using EcoRI and BamHI and the *RPS2* probe was ~545bp fragment cut from pAJ1399 using EcoRI and HindIII. Both probes were gel purified using a Marligen matrix gel extraction kit. Probes were random primed with  $\alpha\text{-}^{32}\text{P}$  dCTP (PerkinElmer) according to Cold Spring Harbor protocols [42] and purified by size exclusion through a 1 ml Bio-Rad Biogel P-20 column using centrifugation. Specific activity of the probes was then assessed by mixing 2  $\mu\text{l}$  of probe with 4 ml Beckman ReadySafe liquid scintillation cocktail and reading the activity using a Beckman Coulter LS 6500 multipurpose scintillation counter. Hybridization was then carried out overnight at 65°C while rotating identically to the pre-hybridization. The next day the hybridization buffer was discarded and the blot was washed in 1x with 100 ml wash 1 (40 mM sodium phosphate pH 7.2, 5% SDS, and 1 mM EDTA) at 65°C for one hour. Wash 1 was then discarded and the blot was then washed 1x with 100 ml wash 2 (40 mM sodium phosphate pH 7.2, 1% SDS, and 1 mM EDTA) at 65°C for one hour. The blot was then removed and placed in a sealable bag with 5 ml wash 2 and placed in a cassette with a Kodak phosphor screen overnight. The next day the phosphor screen was scanned and analyzed using a BioRad Molecular Imager FX and the image was quantitated using ImageJ [43]. ImageJ reports white values so to obtain a band intensity (black value) the value for each band was subtracted from the region just below it to normalize. The resulting values were used to determine an *RPS2/NMD3* ratio.

### **3.6 Genetic test for detection of aneuploidy**

Recombination is suppressed at chromosomal regions genetically linked to centromeres [21]. This fact was used as the basis for a genetic test for the detection of aneuploidy. AJY2685 was mated to AJY2687 and diploids were selected on YPD/G418/Clonat. Diploids were then transformed with pAJ1654 and sporulated. Transformation with pAJ1654 complemented the homozygous *bud23*Δ which was necessary for efficient sporulation. Tetrads were dissected and viable tetrads were then re-streaked onto plates containing 5-fluoroorotic acid to eliminate pAJ1654. Tetrads were then analyzed for the presence or absence of tetratypes. The presence of tetratypes indicates the absence of aneuploidy. See Illustrations 2.1 and 2.2 for a detail of this cross.

### **3.7 Construction of yeast genomic DNA library**

#### **3.7.1 Partial digest and purification of genomic DNA**

100 ml of AJY2683 was grown to saturation in YPD. This culture was then pelleted using a Beckman JA-12 rotor and the pellet stored at -80°C. The pellet was thawed on ice and genomic DNA was extracted according to Cold Spring Harbor protocols [7]. A sample was used to carry out a Sau3AI titration and conditions were chosen to digest the genome to three size ranges bracketing and covering 4-9 kb. Reactions were stopped by the addition of 0.5 M EDTA pH 8.0 to a final volume of 50 mM. These three conditions were used to scale up and digest 4 micrograms of DNA.

These samples were pooled and layered on top of a 5-30% sucrose gradient made in 1 M NaCl, 20 mM Tris-HCl pH 8.0, and 5 mM EDTA pH 8.0. This gradient was then centrifuged for 22 hours at 25°C in a Beckman SW40 rotor at 25,000 RPM. Following centrifugation the gradient was fractionated using an ISCO model 640 density gradient fractionator. 10 ul aliquots of the fractions were separated on a 1% agarose gels in 1x TAE with ethidium bromide and fractions containing 4-9 kb fragments were selected and pooled. Pooled fragments were then extracted 1x with phenol pH 7.9, 1x with 50% phenol pH 7.9/50% 24:1 chloroform:isoamyl alcohol, and 1x with 24:1 chloroform:isoamyl alcohol. Following extraction the pooled fragments were then precipitated by 2x volumes of ice-cold ethanol in the presence of 2 M ammonium acetate pH 5.3. The pellet was washed once with ice-cold 70% ethanol, air dried and resuspended in 100 ul 1x TE.

### **3.7.2 Ligation into vector and purification of the library**

pAJ100 was digested with BamHI, and dephosphorylated with Fermentas shrimp alkaline phosphatase. Next linearized pRS416 was extracted with 50:50 phenol pH 7.9 / chloroform:isoamyl alcohol, and precipitated with 1/10 volume ammonium acetate pH 5.3 and 2 volumes ice-cold 100% ethanol. The pellet was washed once with ice-cold 70% ethanol, air dried and resuspended in 50 ul of 1x TE. The 4-9 kb fragments from the AJY2683 genomic DNA were then titrated into ligation reactions with BamHI cut pAJ100 and conditions were chosen that gave the highest white:blue colony ratio on LB/Ampicillin/IPTG/X-GAL plates in *E.coli* DH5 $\alpha$ . The ligation was then scaled up to

a level that would give at least 5000 white colonies after transformation in order to ensure coverage of the entire *S. cerevisiae* genome. After transformation these colonies were washed off of the LB/AMP/IPTG/X-GAL plates, spun down in a Beckman JA-12 rotor and plasmid DNA was extracted according to standard protocols [36]. Purified library DNA was then resuspended in 200 ul of 1xTE.

### **3.8 Screening of AJY2683 DNA library for genes that improve the *bud23Δ* growth phenotype.**

Library DNA was transformed into AJY2676 and colonies plated to a density of 10,000 colonies per plate on selective media. Out of those plates 300,000 colonies were screened and 300 colonies growing faster than the background colony growth rate were picked. All colonies that reverted to AJY2676 growth after passage through 5-FOA (5-fluorootic acid) plates were selected as candidates. Candidate colonies were then grown to saturation and plasmid DNA was extracted according to standard protocols [36]. The AJY2676 genomic DNA insert was identified as containing *UTP14* using DNA sequencing with M13R and M13F primers and then the rest of the sequencing was completed using AJO1293-1296.

### **3.9 Sequence analysis of *Utp14***

Analysis of Utp14(A758G) by PSI-Blast was identical to the above analysis of Bud23 except that the accession numbers used and data sources were; *Arabidopsis thaliana* NP\_567232, *Danio Rerio* XP\_689811, *Drosophila melanogaster* NP\_648781, *Homo sapiens* AAI22537, *Mus musculus* BAD32202, *Saccharomyces cerevisiae* Utp14 [44], *Schizosaccharomyces pombe* NP\_593375.

### **3.10 Structural prediction of the protein secondary structure around A758.**

Utp14 amino acid sequence was analyzed using the GeneSilico metaserver at <https://genesilico.pl/meta2> [45]. The GeneSilico analysis provided information about putative disordered regions, coiled-coil domains, RNA binding domains, alpha helices, and buried residues. This analysis was accomplished by sending the submitted sequence (the last 500 amino acids of Utp14) to a large number of outside servers that used multiple methods for each kind of prediction, and then provided a consensus prediction where applicable.

## Chapter 4: Results of characterization of Bud23 and phenotypes associated with *bud23Δ* strains

### 4.1 Introduction: Background work

All data in section 4.1 are background material published in White et al, (2008) that were carried out by colleagues (see figure legends) [12]. While validating computational data involving protein interaction maps, Bud23 was identified as a putative small subunit (SSU) biogenesis factor [1]. The evidence for a SSU biogenesis defect was obtained by comparing WT and *bud23Δ* strains using polysomal analysis (Figure 4.1, [12] ) and northern blots (Figures 4.2, 4.3, [12] ) probing for specific rRNA processing intermediates in ribosome biogenesis. On the WT polysomal profile, from left to right peaks represent molecules with progressively greater mass. Starting from the left, the peak representing the 40S ribosomal subunit appears first, followed by the 60S ribosomal subunit, a large 80S ribosome, and then polysomes representing 2 ribosomes on mRNA, 3 ribosomes on mRNA and so on. In a *bud23Δ* strain the 40S peak essentially disappears, the 60S peak increases greatly, the 80S decreases significantly, and there is a general decrease in the number of polysomes. The drop in 40S, 80S, and polysomes, and increase in 60S implies that there are fewer 40S subunits available in a *bud23Δ* mutant to pair with the available 60S particles. Disassociating all ribosomes under high salt conditions revealed a clear subunit imbalance when comparing WT (Figure 4.1 upper right, [12] ) and *bud23Δ* strains (Figure 4.1 lower right, [12]). The WT ratio of 40S peak to 60S peak

was 0.59, and when *BUD23* is deleted the ratio moved to 0.185 due to a significant drop in 40S levels.

The northern blot analysis confirmed the biogenesis defects at the level of steady state rRNA. Figure 4 shows a schematic of the 35S rRNA with a detail of the region between the D and C1 site cleavages. Small bars labeled a-h represent probes used to detect specific rRNA processing intermediates and the intermediates themselves are aligned next to each band on the northern blot (Figure 4.3, [12] ). Starting at the beginning of processing, a large increase in the level of 35S rRNA is seen in the *bud23Δ* strain relative to WT. Accumulation of 35S is a common feature of small subunit biogenesis defects and is thought to be a result of slowed processing [12, 13, 46]. A large drop in the level of 27S and 27SA precursors of the 25S is also seen in *bud23Δ* relative to WT. This is thought to be an indirect effect of the defect in 40S biogenesis [12]. When the 20S and 18S precursor rRNAs are examined, a decrease in the level of 18S and an increase in the level of 20S is observed in the *bud23Δ* strain. The drop in levels of 18S is consistent with the decrease in the level of 40S in the polysome profile. However the 20S increase suggests a late stage defect in 40S production (pre-40S) as earlier precursor particles tend to be rapidly degraded [47]. This result inspired an analysis of the localization of small ribosomal proteins fused to GFP (Figure 4.4, [12] ). In WT cells Rps2-GFP is localized throughout the cytoplasm. In *bud23Δ* cells there is an accumulation of Rps2-GFP in the nucleus, relative to WT. When compared with a nucleolar marker (Sik1-mRFP) it can be seen that the accumulation is truly nuclear and not nucleolar as is typical with small subunit biogenesis defects.

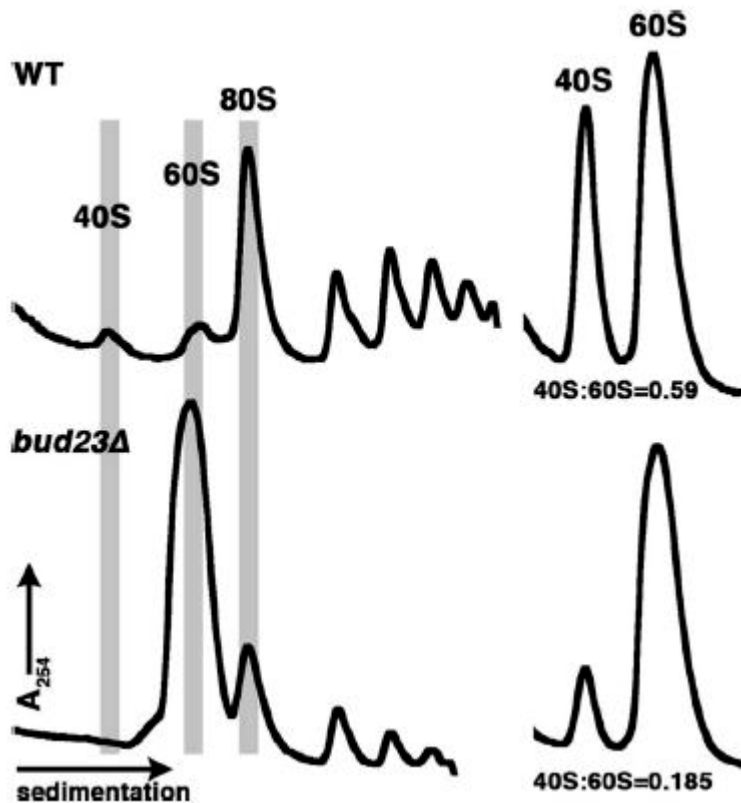


**Figure 4.1: Polysomal and subunit analysis of WT and *bud23Δ* strains (White et al 2008, work by Richa Sardana).**

WT and *bud23Δ* yeast were harvested during exponential growth. For polysomal analysis yeast were treated with cyclohexamide and protein extracts analyzed as outlined in White et al, 2008. For subunit analysis polysomes were dissociated under high salt and analyzed as outlined in White 2008. A WT polysomal profile (top left) and subunit ratio (top right) was compared to a *bud23Δ* polysomal profile (bottom left) and subunit ratio (bottom right). *bud23Δ* cells display; lower 40S, 80S and polysomes, higher 60S, and a decreased 40S:60S ratio when compared to WT.

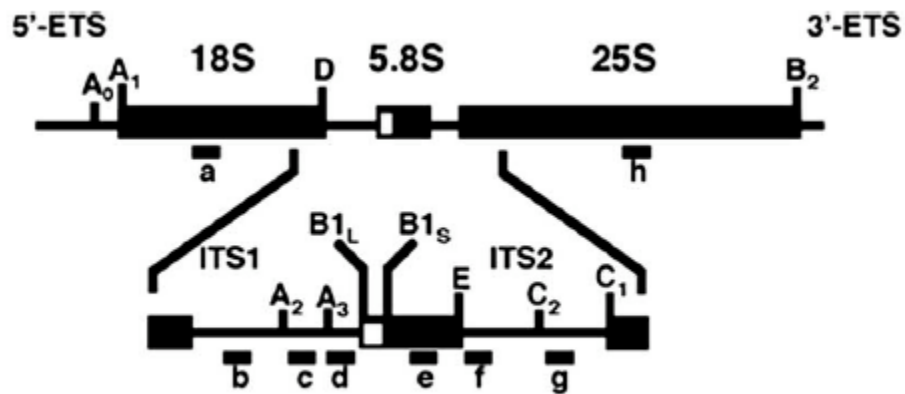


**Figure 4.2: 35S rRNA diagram with a detail of the ITS1 region showing northern blot probe sites (White et al, 2008, work by Zhihua Li).**

The position of oligonucleotides used as probes for northern blotting in Figure 4.3 and indicated by bars and labeled alphabetically.

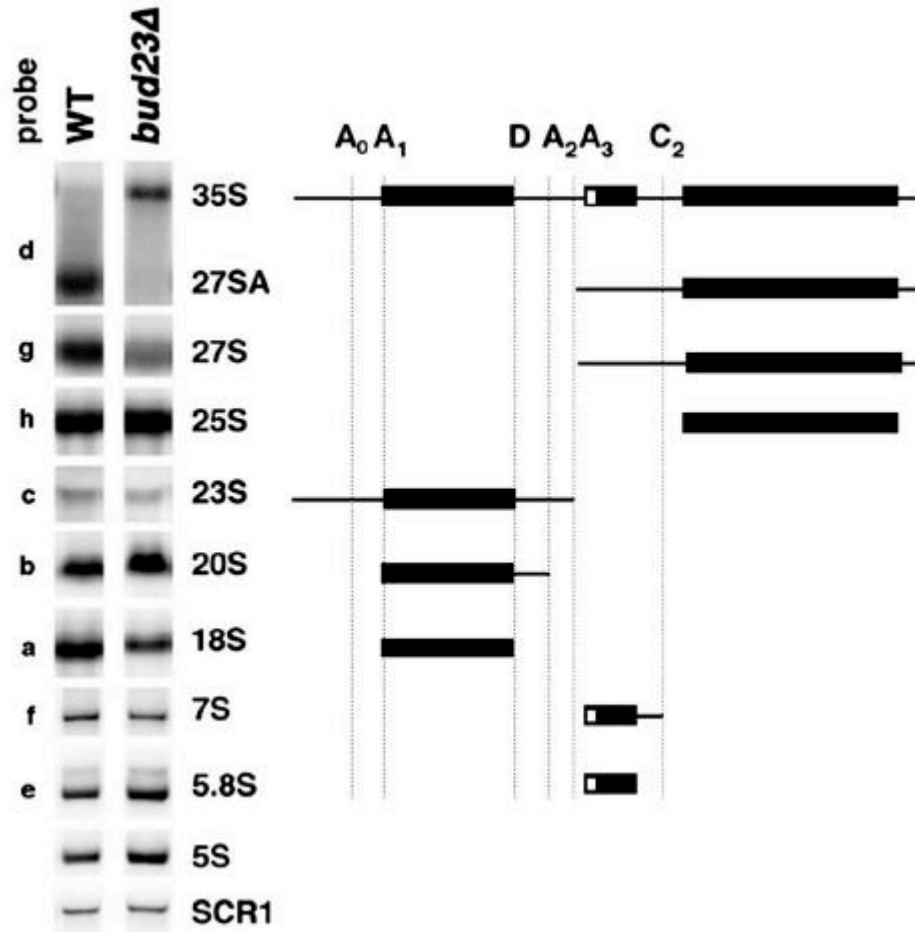


**Figure 4.3: Northern blotting of rRNA processing intermediates in WT and *bud23Δ* cells (White et al, 2008, work by Zhihua Li).**

Total RNA was prepared, blotted, and probed with oligonucleotides as indicated in figure 4.2. Probes and corresponding processing intermediate are indicated. *bud23Δ* cells display decreased 18S, and an increased 20S in comparison with WT. *bud23Δ* cells also display decreased 27S and increased 35S. SCR1 is included as a loading control.

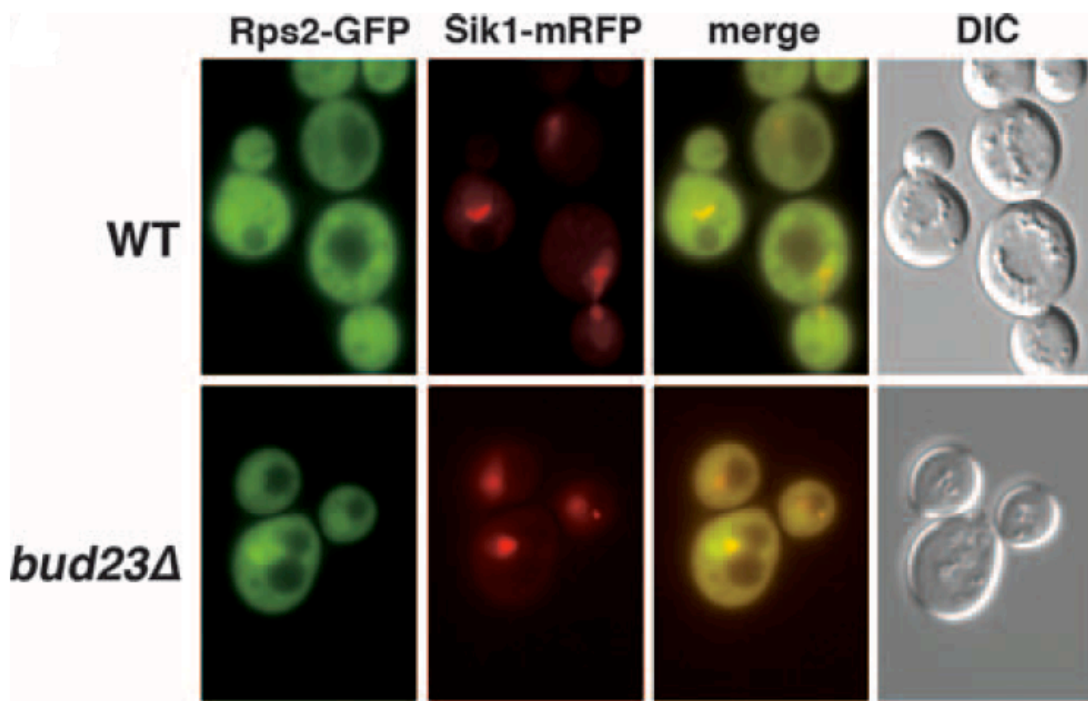


**Figure 4.4: localization of an Rps2-GFP reporter in WT and *bud23Δ* cells (White et al, 2008, by Arlen Johnson).**

WT (top) and *bud23Δ* (bottom) cells were transformed with plasmids expressing Rps2-GFP (pAJ1399) and Sik1-mRFP (pAJ1629) and visualized by fluorescence microscopy. Sik1-mRFP is a nucleolar marker. Comparison of the merged images demonstrates that Rps2-GFP accumulates in the nucleus of *bud23Δ* cells (bottom, merge) compared to WT (top, merge) cells.

## **4.2: Fluorescent in situ hybridization of ITS1 confirms nuclear accumulation of pre-40S ribosomal subunits**

While the Rps2-GFP localization data seemed to indicate a nuclear mislocalization of Rps2-GFP, there is an objection to the data that requires a second approach to validate the result. An alternate interpretation is that Rps2-GFP may not be efficiently incorporated into pre-40S particles in a *bud23Δ* mutant and therefore the accumulation represents free Rps2-GFP and not pre-40S particles. Therefore fluorescent in-situ hybridization (FISH) was used to localize the 20S rRNA in *bud23Δ* AJY2161 cells. Figure 7 shows the result of FISH using Cy3 labeled AJO1024 which is complementary to ITS1. The data is compared to two control strains. The first is a WT control. The second is AJY1539, a strain expressing a mutated version of Crm1 (*crm1(T539C)*) which is sensitive to the drug leptomycin-B (LMB). Exposure to leptomycin-B results in blockage of nuclear export of all cargos dependent on Crm1 for export, including ribosomes. These strains were also all stained with DAPI to visualize genomic DNA. The WT strain displayed localization of 20S identical to what has been described previously (Figure 4.5, top left [12]) [13]. A crescent shaped nucleolar localization spatially separate from the genomic DNA with a very faint ITS1 signal throughout the rest of the cell was observed. AJY1539 looked similar to the WT strain without LMB exposure (Figure 4.5, top right [12]). When AJY1539 is exposed to LMB however the Cy3 signal intensifies in the nucleus as shown by the observation that the genomic DNA region takes on a slight purple quality and the red can be seen extending

out to the nuclear periphery. There is also a slight drop in the level of cytoplasmic ITS1 (Figure 4.5, bottom right [12]). When these controls are compared to the *bud23Δ* strain an intense increase in the nucleolar Cy3 signal is observed, the genomic DNA signal is clearly purple, there is clear ITS1 staining out to the nuclear periphery, and the cytoplasmic ITS1 signal has disappeared (Figure 4.5, bottom left [12]). The blue to purple shift of the nucleoplasm indicates that there is a nuclear accumulation of 20S rRNA. Altogether the data in Figure 4.5 supports the view that in a *bud23Δ* mutant a late stage pre-40S particle accumulates in the nucleus.

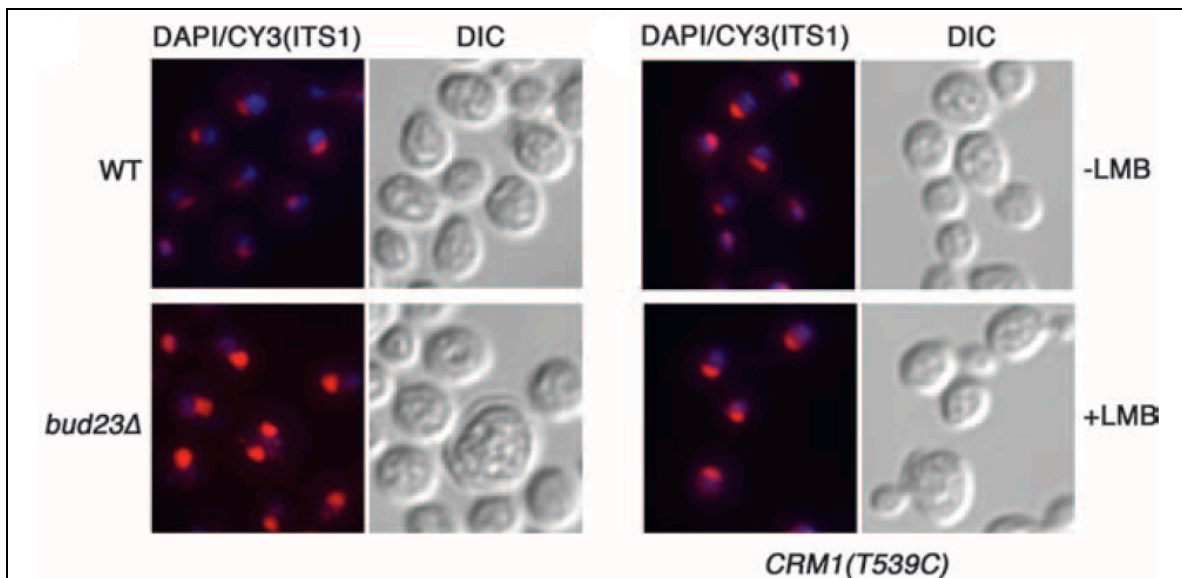
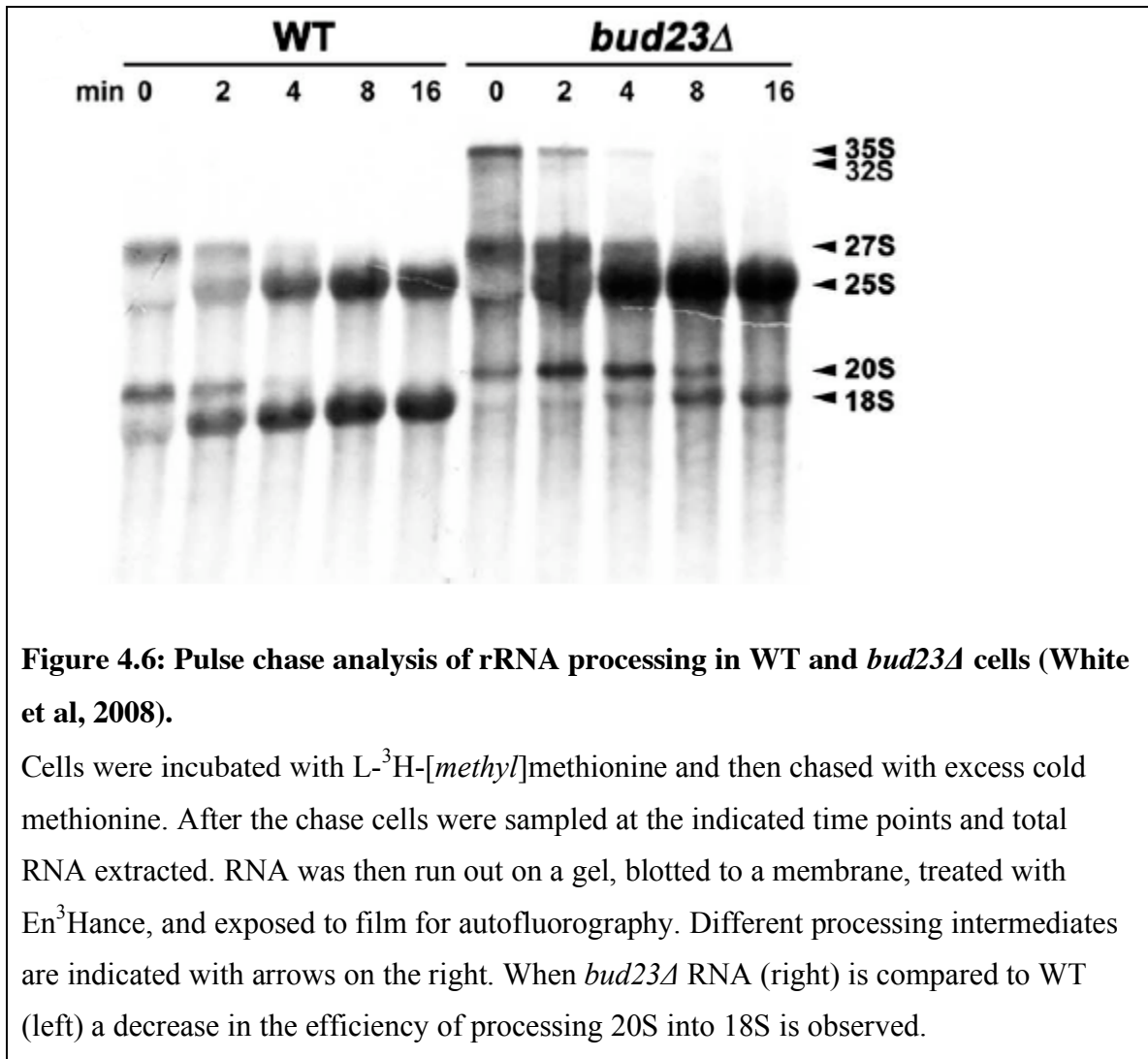


**Figure 4.5: Comparison of localization of ITS1 in WT and *bud23Δ* cells (White et al, 2008).**

Fluorescent in-situ hybridization of a Cy3 labeled oligonucleotide was used to localize ITS1 in both WT (top left) and *bud23Δ* cells (bottom left). As a comparison Leptomycin-B sensitive AJY1539 (*crm1T539C*) (LMB- top right, LMB+ bottom right) was used as a control to demonstrate the localization ITS1 in of a strain that was known to be defective in small subunit export. *bud23Δ* cells show an accumulation of ITS1 in the nucleus and a drop in the cytoplasm when compared to WT cells.

### **4.3: L-<sup>3</sup>H-[methyl]methionine pulse chase labeling demonstrates defects in 18S formation**

In the *bud23Δ* AJY2161 mutant the steady state level of 20S is increased and the level of 18S is decreased relative to WT strains. A standard way of analyzing the kinetics of 35S processing into mature rRNA is pulse labeling of the rRNA with radiolabeled S-adenosylmethionine (SAM). Cells use SAM as the methyl donor in the methylation of rRNA [48]. WT and *bud23Δ* strains were pulse labeled with L-<sup>3</sup>H-[methyl]methionine and then chased with excess unlabeled methionine, and the labeled rRNA was followed over a period of 16 minutes (Figure 4.6 [12]). The WT strain (Figure 4.6, left [12]) showed rapid incorporation of label in 20S, and a fraction of 18S at the 0 time point. Most of the labeled 20S was completely processed into 18S at 4 minutes, and was completely processed by 8 minutes. There was no visible label remaining in 20S at the 16 minute time point. The *bud23Δ* strain in contrast (Figure 4.6, right [12]) showed a similar level of 20S labeling at the 0 time point, but almost no labeling of 18S. At the 4 minute time point most of the small subunit rRNA was still present as 20S and it was not until 16 minutes that most of the 20S was processed into 18S. In fact the 4 minute WT and the 16 minute *bud23Δ* samples look very similar. Also of note was the accumulation of 35S rRNA which is common in small subunit biogenesis defects. No significant effect on 60S processing was observed. This pulse chase of the *bud23Δ* strain is strikingly similar to deletions of other proteins important for the export of the small subunit including Yrb2 [49] and Rrp12 [50].



#### **4.4.1: Justification for analyzing methylation of m<sup>7</sup>G1575 in *bud23Δ* cells**

Sequence analysis of Bud23 using NCBI PSI-BLAST revealed that Bud23 was very highly conserved among eukaryotes and was putatively an S-adenosylmethionine dependant methyltransferase (Figure 4.7) [34]. More specifically, a NCBI protein blast search indicates the Bud23 methyltransferase domain has homology to the Rossmann super family of methyltransferases. The blast list of domain hits indicates that many members of this family seem to act on small molecules such as ubiquinone [12]. However, outside of the highly conserved methyltransferase domain (approximately residue 50-160 on Bud23), no putative domains are detected. This region outside of the methyltransferase domain is rich in positively charged amino acids which would be expected of a protein that would need to bind a negatively charged rRNA. Examination of the data on known methylations of the 18S rRNA at the University of Massachusetts Amherst “3D Ribosomal Modification Maps” [35] was then carried out (Arlen Johnson, personal communication). This analysis revealed that only one methylation of the 18S had an unknown methyltransferase, the 7-methylguanine present at G1575.



NCBI PSI-BLAST was used with the Bud23 amino acid sequence to find homologous proteins in other organisms. These sequences were then analyzed with a CLUSTAL W2 sequence alignment program. Amino acids are grouped by color; red= small, blue = acidic, magenta= basic, green= Hydroxyl + Amine + Basic - Q.

#### **4.4.2: Primer extension analysis reveals that 18S rRNA G1575 is not methylated in a *bud23Δ* strain**

RNA base modifications are routinely detected using primer extension. Briefly, reverse transcriptase will continue along an unmodified RNA molecule until the end, but a modification will tend to stop the reverse transcriptase, producing an additional smaller product on a DNA gel when compared to DNA from an unmodified template RNA.

Primer extension was carried out on total RNA samples from both WT and *bud23Δ* AJY2161 cells. A primer (AJO1027) that binds downstream of G1575, but upstream of the dimethylation at A1518 and A1519 was used for the reverse transcription reaction. A useful marker for this work was a 2'-O-methylation at position G1572 directed by the binding of the snR57 guide RNA [35]. When primer extension was carried out on WT total RNA strong-stops were visible at 62 (G1575) and 65 (G1572) bases in size (Figure 4.8). When primer extension was carried out in a *bud23Δ* strain, only the 65 nucleotide product indicative of the G1572 modification was present. The clear lack of a stop at 1575 in the deletion strain relative to the WT strain strongly suggests that without Bud23, G1575 can not be methylated.

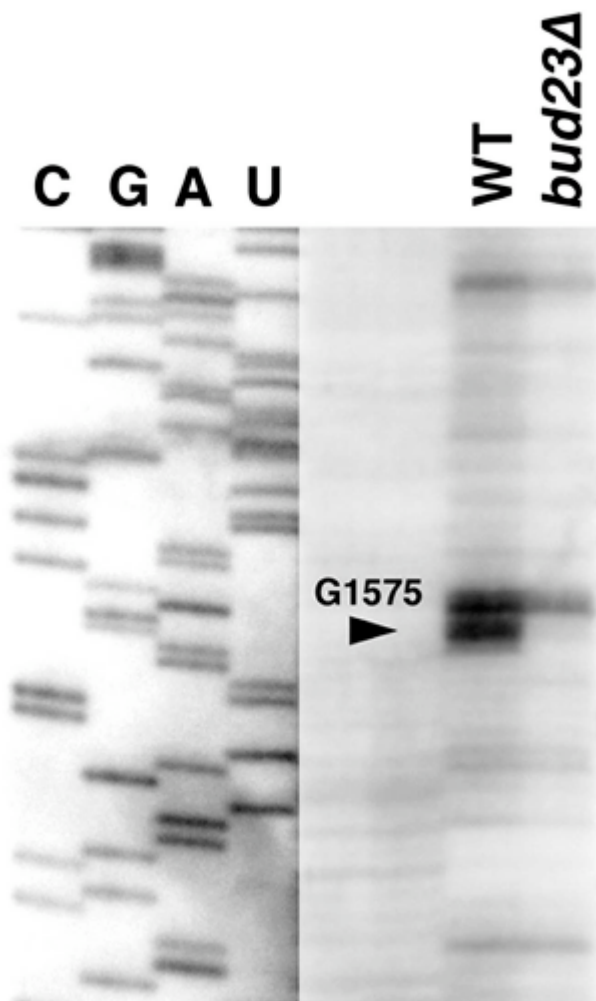


**Figure 4.8: Primer extension of small subunit rRNA reveals lack of methylation at G1575 in a *bud23Δ* strain**

Total RNA from WT and *bud23Δ* strains were used in primer extension reactions using primers that bound downstream of G1575. These primer extension reactions were run alongside DNA sequencing reactions using the same primer on an rDNA locus. When comparing the WT lane with the *bud23Δ* lane the band corresponding the m<sup>7</sup>G1575 is noticeably absent in the *bud23Δ* lane.

#### **4.4.3: m7G1575 cleavage supports primer extension data that Bud23 is necessary for methylation at G1575.**

While the results of the primer extension were encouraging, traditionally m7G modifications are difficult to detect by primer extension [51]. In order to be sure of these results a technique was used that specifically cleaves RNA at m7G (Figure 4.9) [38]. In addition, G1575 methylation was assessed in *bud23* mutants predicted to be methyltransferase-deficient (Figure 4.9) [12, 48].

Total RNA was extracted from *bud23Δ* (AJY2161) yeast that contained either pAJ99 (empty vector), pAJ2154 (*BUD23*), or mutant versions of *bud23*, and then cleaved at 7-methylguanines by sodium borohydride/aniline treatment. When the *BUD23* yeast RNA was used for primer extension similarly to the WT above, a strong stop was visible for G1575. In the same sample the stop at G1572 was virtually undetectable. This is because if most of the rRNA is cleaved at m7G1575 the reverse transcriptase cannot proceed to G1572. When the empty vector *bud23Δ* strain RNA was analyzed the strong stop at G1575 disappeared and the stop for G1572 greatly intensified indicating the RNA was not cleaved at G1575 and the reverse transcriptase was able to read through to G1572. This result validates the result obtained with primer extension alone.

One possible alternate explanation to the above results is that Bud23 is important for the methylation at G1575 but is not itself the methyltransferase. To investigate this

methylation of G1575 was assessed in mutants predicted to be deficient in methyltransferase activity using the same sodium borohydride cleavage assays. pAJ2155 and pAJ2156 contain the mutants *bud23(D77K)* and *bud23(G57E)* respectively. Strains that are *bud23Δ* (AJY2161) and contain these plasmids grow at virtually the same rate as a WT strain that contains an empty vector (Figure 4.10) [12]. When total RNA is extracted from these strains and analyzed by sodium borohydride cleavage and primer extension they display the same cleavage as the *bud23Δ* strain that contains empty vector. The G1575 stop is not visible and the G1752 stop is present indicating reverse transcriptase reads past the potential cleavage site. These results suggest that Bud23 is the methyltransferase directly responsible for m7G1575.

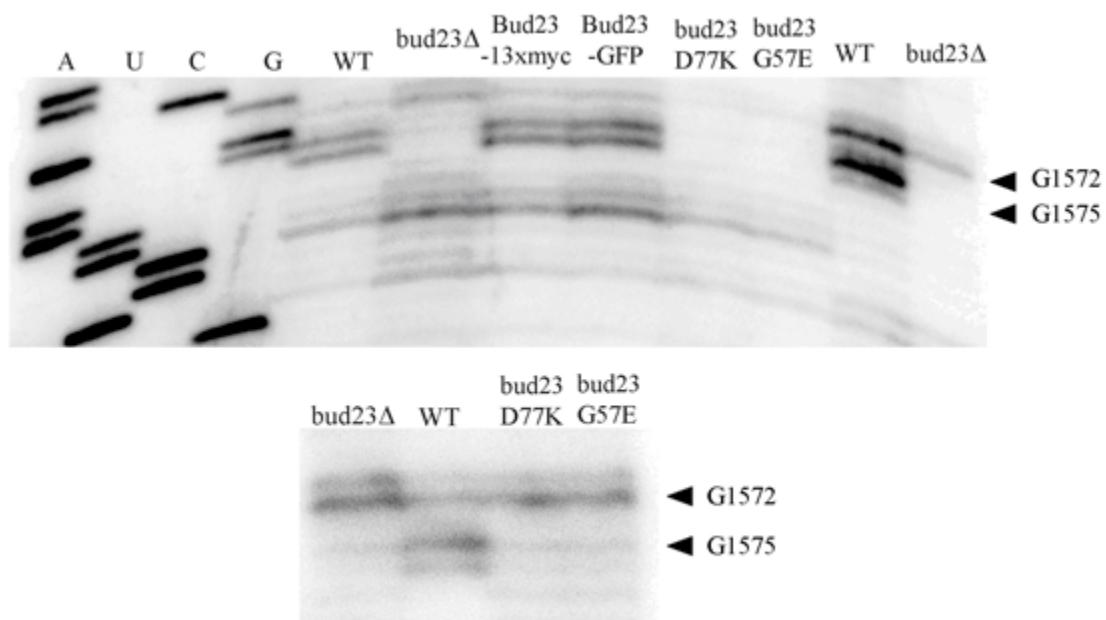


**Figure 4.9: Primer extension of small ribosomal rRNA following sodium borohydride/aniline cleavage confirms that *bud23Δ* strains lack m7G1575**

Total RNA from strains was subjected to cleavage at m7G by sodium borohydride and aniline followed by primer extension. WT strain was BY4741 containing empty vector (pAJ99). All other strains were *bud23Δ* strains containing either empty vector (always pAJ99 here) or expressing the indicated form of Bud23. *bud23(G57E)* (pAJ2155), *bud23(D77K)* (pAJ2156), *BUD23-13xmyc* (pAJ2163), *BUD23-GFP* (pAJ2151). WT cells or *bud23Δ* cells expressing fusions of Bud23 with a 13xmyc epitope or GFP contain m7G at 1575. RNA from strains where Bud23 is deleted or where a methyltransferase deficient form of bud23 is expressed is not methylated at G1575.

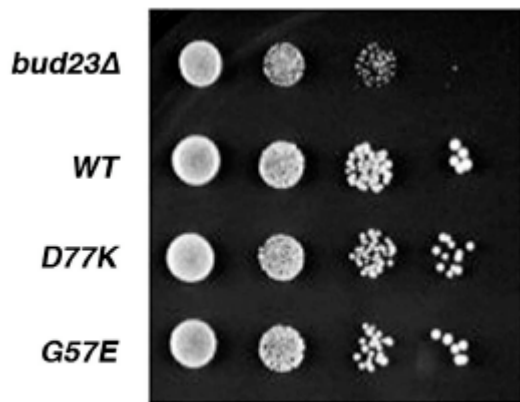


**Figure 4.10: expression of methyltransferase deficient *bud23* recovers growth of *bud23Δ* to nearly WT levels [12]**

*bud23Δ* deletion strain AJY2161 was transformed with plasmids pAJ2155 (*bud23(D77K)*) or pAJ2156 (*bud23(G57E)*) and compared to WT (AJY2161 + pAJ2154) or AJY2161 containing empty vector. When compared to WT and *bud23Δ* strains, the methyltransferase deficient strains grow slightly slower than wild type.

## 4.5: Discussion

### *bud23Δ* strains display pre-40S export defects

Previous work with an Rps2-GFP reporter suggested that the accumulation of 20S and drop in 18S in a *bud23Δ* mutant was due to an export defect that caused an accumulation of pre-40S particles [12]. Pre-40S particles trapped in the nucleus would be unable to undergo cleavage at site D and become mature 40S particles. Fluorescent in-situ hybridization using a probe specific for ITS1 confirmed the Rps2-GFP result revealing a nuclear accumulation of ITS1 and showing that both the protein and rRNA components of pre-40S accumulate (Figure 4.5). This nuclear accumulation is significant because earlier defects in the production of small subunits result in nucleolar accumulation of pre-40S. This is a consequence of the fact that as the 35S is processed, small subunit proteins and biogenesis factors bind and form the 90S and the pre-40S is the first product of ribosome biogenesis [12, 13, 46]. Once the A2 cleavage occurs, a relatively simple pre-40S particle rapidly moves from the nucleolus through the nucleoplasm to be exported. Based on these results, it is this window from A2 cleavage through export where Bud23 likely plays its role. The deletion of Bud23 also causes the accumulation of 20S in the nucleolus which suggests that Bud23 binds and plays a role in that compartment. It is notable that the Rps2-GFP localization did not show nucleolar accumulation when *BUD23* was deleted. This may mean that this reporter was not binding to pre-40S particles in the nucleolus, and that Bud23 may be important for the proper binding of Rps2.

The results from the pulse-chase analysis (Figure 4.6) are consistent with the northern blot and FISH analysis (Figure 4.5). *bud23Δ* strains display reduced flux through small subunit processing. 20S becomes methylated rapidly, similar to WT, but the labeled 20S then takes much longer to process into 18S than in the WT strain, perhaps as much as four times as long (figure 6). This is very similar to the situation with Yrb2 and Ltv1 [13, 49]. Yrb2 and Ltv1 are two proteins that function in pre-40S export whose deletion mutants also display nuclear accumulation of pre-40S particles and slowed processing of 20S into 18S [13, 49]. Yrb2 interacts with Crm1 and thus is very likely to be part of the system that small subunits use for export [49].

### **Bud23 is required for m<sup>7</sup>G1575 of the 18S**

From earlier work Bud23 was predicted to be a methyltransferase by amino acid sequence homology [48]. Previous to our work on Bud23 considerable analysis of the position and identity of most rRNA modifications had already occurred. In this dataset, one methylated guanine in the 18S had no associated methyltransferase [35], the 7-methylguanine at position 1575. While it was possible that Bud23 was methylating a protein or other substrate, an analysis of Bud23 sequence outside of the conserved methyltransferase domain revealed a large number of positively charged residues (lysines and arginines). Protein domains that bind nucleic acids tend to be basic (histones for example) so it seemed worth while to look for a connection between Bud23 and rRNA methylation.

Primer extension is a useful technique for the detection of modified RNAs because a modification can stop reverse transcription. Primer extension on WT 18S revealed two strong stops in the vicinity of G1575 (Figure 4.8). There are two modifications in this region, the 2-O-methylation at G1572 and the m<sup>7</sup>G1575. When *BUD23* is deleted the stop at G1572 disappears. This is good evidence supporting a role for Bud23 in the methylation of G1575.

There are a couple of objections to the above data however. One objection involves the fact that it is difficult to detect a 7-methylguanine using primer extension [51], because the methylation does not occur at an amine involved in base pairing with the cytosine (Illustration 4.1). However we clearly detect a stop at G1575. I favor the view that the presence of the 2'-O-methyl group at G1572 creates synergy in the disruption of reverse transcriptase processivity allowing primer extension greater sensitivity to m<sup>7</sup>G in our case. However we decided to analyze methylation at G1575 by a different method in order to increase our confidence in these results. It has been known for some time that m<sup>7</sup>G can be specifically cleaved by reduction with sodium borohydride and cleaving of the backbone with aniline [38]. I combined this technique with primer extension to enable more confident detection of the modified base (Figure 4.9). This experiment showed that cleavage did not occur at G1575 when *BUD23* was deleted demonstrating that G1575 was not methylated.

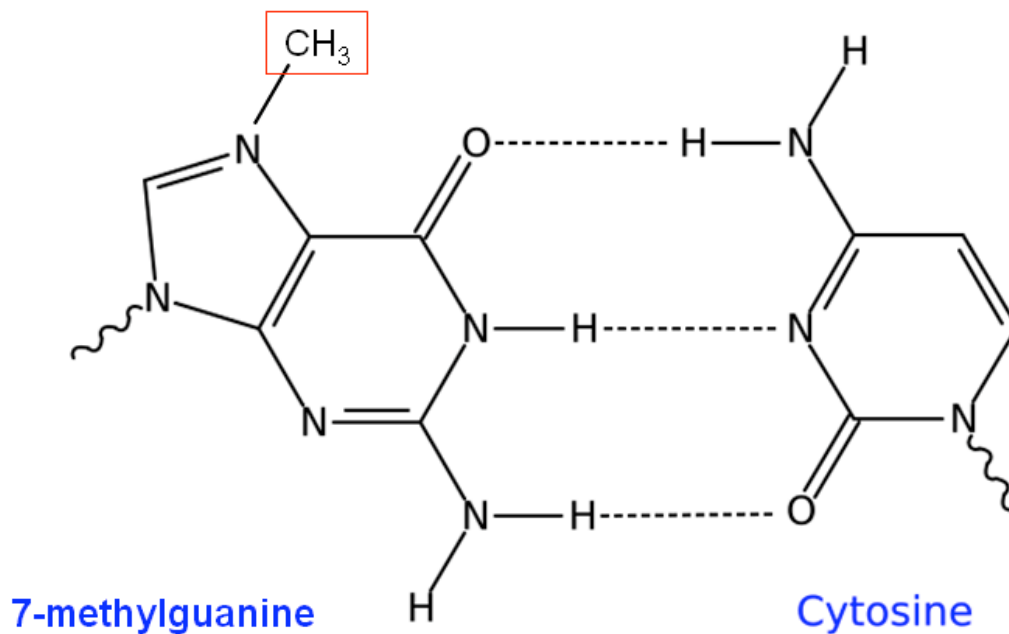


**Illustration 4.1: Diagram of a CG base pair**

The position methylated by Bud23 is the N7 position of the guanine (left) base. Note that the N7 nitrogen is not involved in base pairing.

### **What is the role of Bud23 in ribosome biogenesis and function?**

The methylation carried out by Bud23 seems dispensable for the normal production and function of ribosomes under the tested conditions. This puts the m7G1575 in the same category as all other rRNA modifications, its role in biogenesis and function of ribosomes remains unknown. Individually the loss of m7G has no significant phenotype as has been previously observed in mutants for the production of other modifications. However, it is possible that the slight growth phenotype of the *bud23(G57E)* and *bud23(D77K)* may represent a real effect of m7G1575. If this is the case this may indicate that the m7G1575 may have a more severe phenotype than most rRNA modifications. Within the context of G1575 it may be worth considering that lack of methylation may lead to other phenotypes. G1575 is located on a base that projects directly towards the tRNA anticodon loop in the P-site. While the methylation itself faces away from the tRNA, it is possible that the Bud23 methylation has subtle effects on translation that are not visible under the growth conditions tested. Previous work has demonstrated that preventing individual modifications can increase or decrease growth rate under specific growth conditions or environmental challenges [25]. Additionally the proximity of G1575 to the decoding center may put it in a position to affect the translation of specific classes of mRNAs, or methods of translational regulation such as IRES containing mRNAs. Also lack of G1575 may possibly affect sensitivity to antibiotics that bind near the decoding center. Future work will be able to test these hypotheses.

Since the methylation is dispensable, what role Bud23 plays in ribosome biogenesis must be defined. The localization of Bud23-GFP is nuclear with a nucleolar focus [12]. Western blots of polysomal fractions from Bud23-GFP using antibodies against GFP show that Bud23 sediments with the free 40S as well as with 90S particles (Richa Sardana, personal communication). In addition, *RPS2* was identified as a high copy suppressor of *bud23Δ* (Figure 4.11). The above additional data indicate that Bud23 may bind in the nucleolus around the time when the A2 cleavage occurs. Since over-expression of Rps2 improves growth a reasonable hypothesis is that the binding of Bud23 helps to guide the later stage folding of the pre-40S just before or during the binding of Rps2 (they may bind sequentially or simultaneously). Without Bud23 the structure of the pre-40S may take longer to achieve a proper configuration conducive to Rps2 binding. If extra Rps2 is available during a transition to a more mature conformation, it can bind and biogenesis will continue.

This whole process probably also impacts nucleolar export since in *S.pombe* depletion of Rps2 leads to nucleolar accumulation of 20S, where here deletion of *BUD23* leads to a nucleolar and nuclear accumulation [52]. Assuming conservation of biogenesis pathways, if binding of Rps2 is necessary for nucleolar export, anything that results in more bound Rps2 could improve SSU biogenesis. This delay in the nuclear and cytoplasmic localization of pre-40S is consistent with the fluorescent in situ hybridization data (Figure 4.5) since an increase in the intensity of the nucleolar ITS1 signal is seen alongside the nuclear accumulation. This would lead to an accumulation of 20S in general, and presumably delay incorporation of factors important in the export of the pre-40S. This putative role for Bud23 would be a chaperone that aids in the structural

changes necessary binding of Rps2, *and* binding of export factors. Such changes in structure between WT and deletion of Bud23 could be detectable through assays sensitive to changes in accessibility of regions of the 18S backbone such as DMS foot printing.

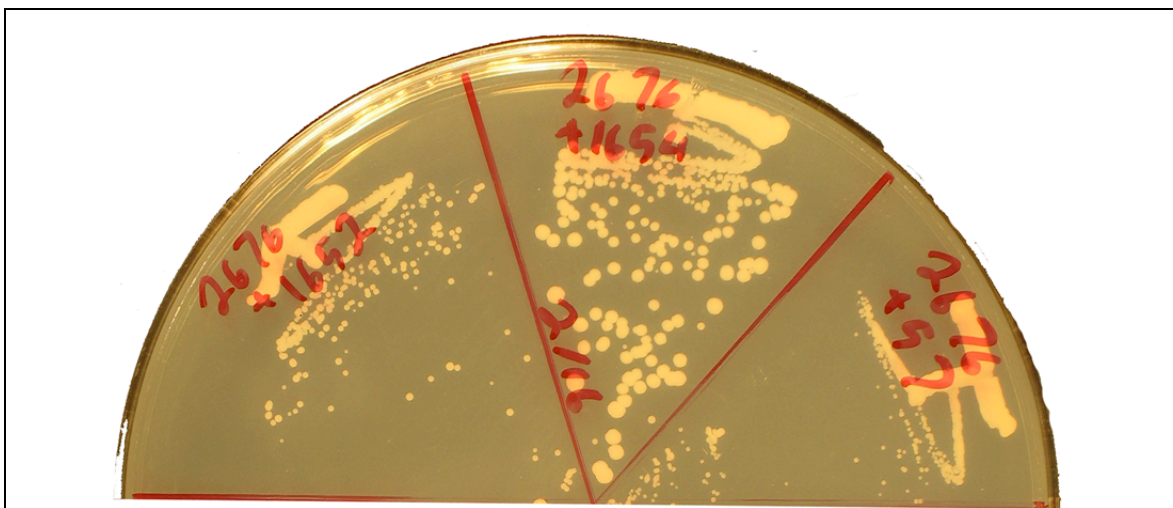


**Figure 4.11: Suppression of the *bud23Δ* growth phenotype by over-expression of Rps2.**

*bud23* deletion strain AJY2676 was transformed with empty (pAJ57), WT *BUD23* (pAJ1654), or *RPS2* (pAJ1652) 2 $\mu$  multicopy expression vectors. The over expression of Rps2 slightly improves the growth rate of a deletion strain.

## **Chapter 5: Identification and characterization of dominant suppressors of *bud23Δ*.**

### **5.1: Background**

During the work that lead to the previous chapter of this thesis it was noticed that faster growing colonies would often appear in freshly streaked stocks of *bud23Δ* strains. It was hypothesized that we were observing suppressor mutants of the *bud23Δ* growth phenotype. The *bud23Δ* strain is a slow growing strain. Any yeast cell within this population that received a mutation enabling it to grow better than the rest of the culture would be at a selective advantage. Identifying such a suppressor mutant could inform us of the function of Bud23 in ribosome biogenesis.

### **5.2: UV mutagenesis of the *bud23Δ* strain AJY2676.**

AJY2676 was grown in liquid culture to an  $A_{600}$  of ~0.4. This culture was split into 4 samples and each was given increasing amounts of UV exposure or no UV exposure. The sample with the lowest amount of UV exposure was the one with the desired 10% survival rate. When this culture was then grown on plates as a dilute lawn of ~8000 colonies per plate, nineteen colonies that grew better than the parental AJY2676 were picked, re-streaked, patched and frozen at -80°C (Figure 5.1). One UV mutant colony that grew particularly well (#8) was chosen for further analysis and named AJY2684. When the un-exposed culture was plated similarly it was discovered that there was already a suppressor mutant present in the AJY2676 culture when the UV mutagenesis was carried out. Therefore some of the UV mutants are likely the same

suppressor as the spontaneous suppressor in the untreated sample. Eight of these spontaneous suppressor colonies were picked, and two are shown in Figure 12 (S1 (AJY2683), S2), but all spontaneous suppressors grew at an identical rate (data not shown) making it possible that they represent the same mutation. In order to be sure of my isolation of a spontaneous suppressor from a *bud23Δ* strain PCR was carried out on genomic DNA from the suppressors, AJY2676, and controls using a forward outside primer specific to Bud23 promoter sequence (AJO1035), and a reverse internal primer specific to the NatMX gene (AJO786). The results of this PCR confirmed the presence of the *bud23Δ* locus (Figure 5.2).

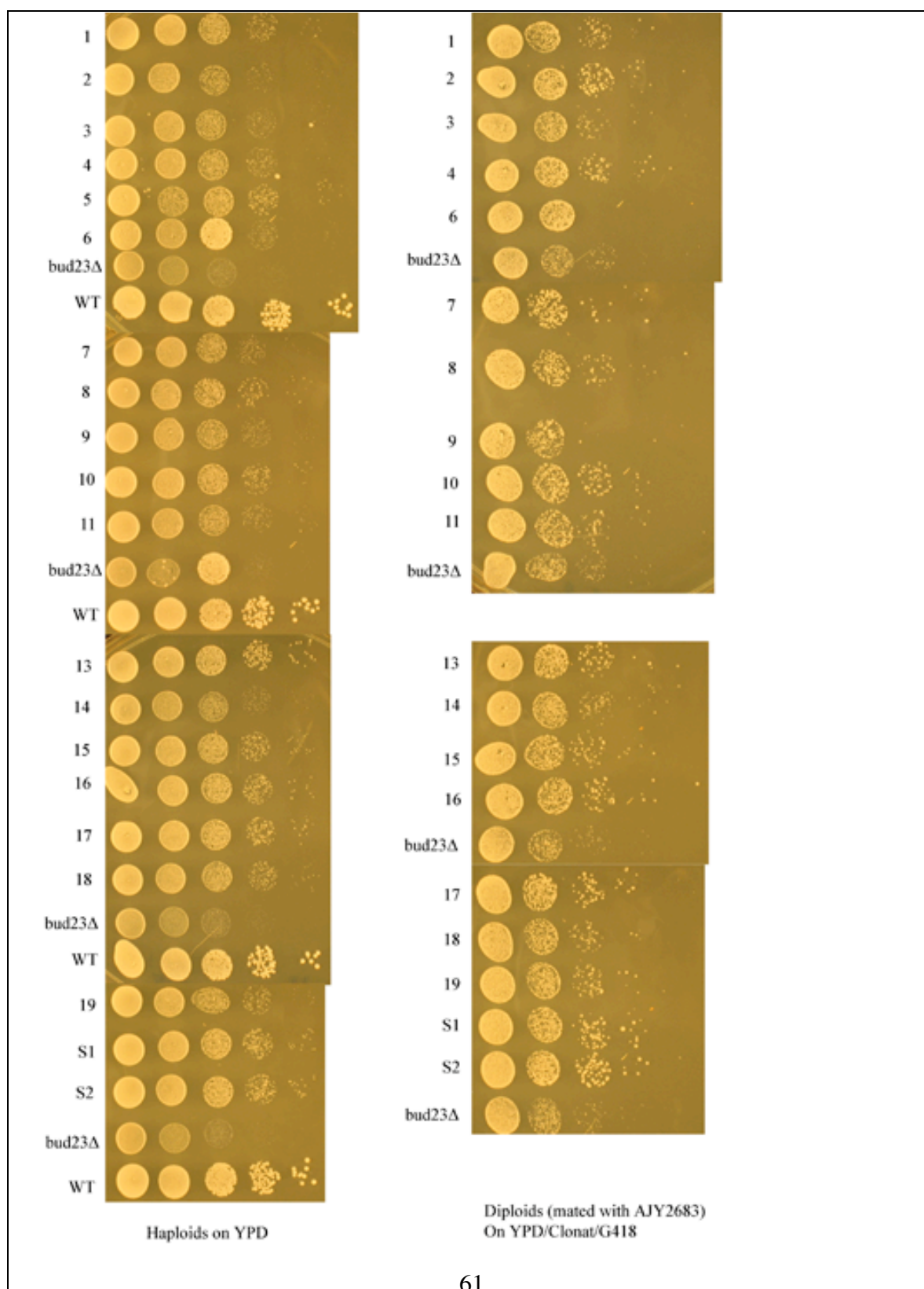
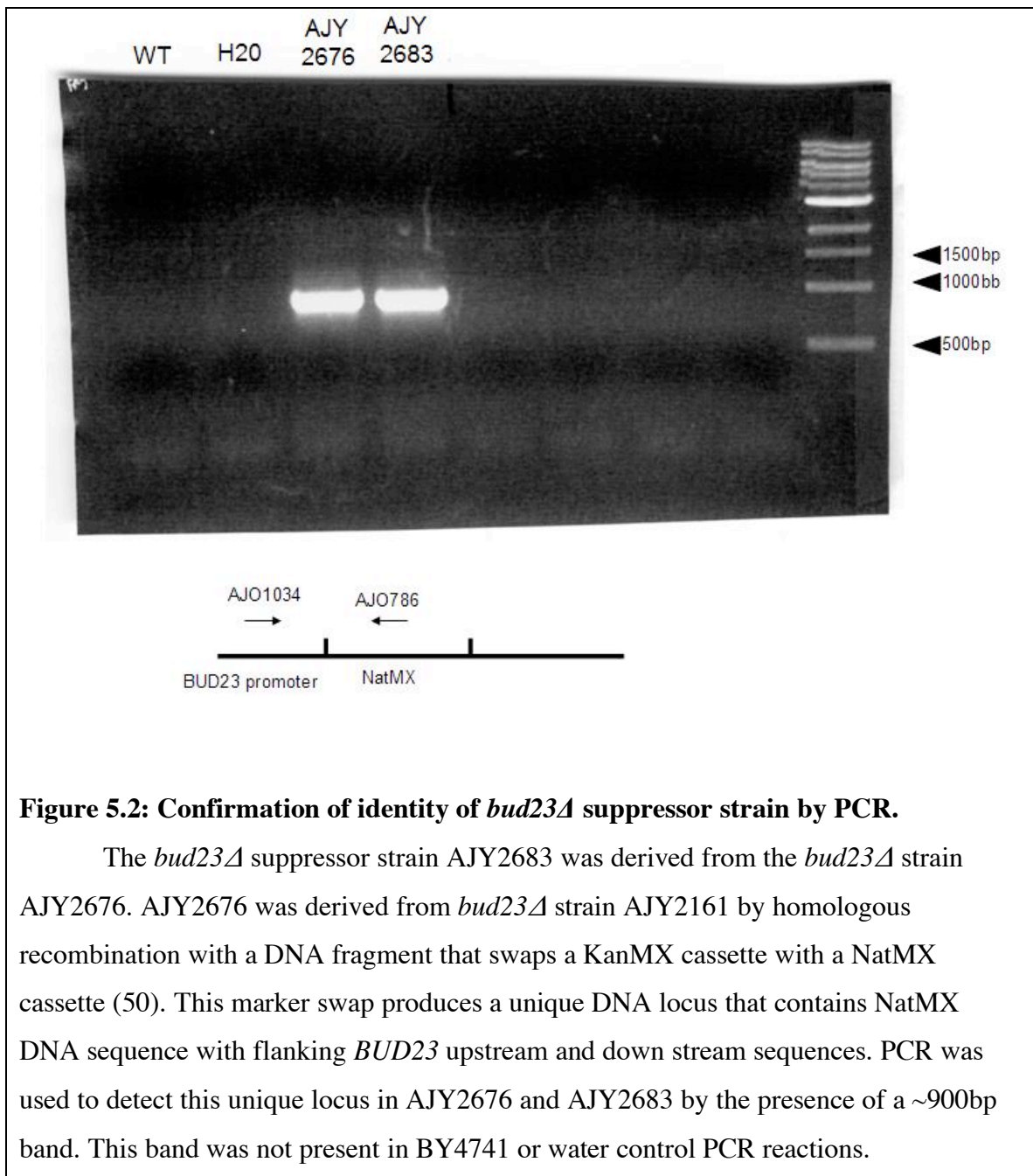


**Figure 5.1: Mutants that suppress the *bud23Δ* phenotype**

A *bud23Δ* culture was mutagenized with UV radiation and fast growing colonies were isolated (1-19). Fast growing colonies that were present in the sample unexposed to UV radiation were saved as spontaneous suppressors (S1, S2). Haploid suppressor mutants are compared with WT and normal *bud23Δ* strains on YPD on the left. Diploid suppressor mutant strains produced by mating haploids with AJY2683 are plated on YPD/clonat/G418 with a normal *bud23Δ* diploid strain on the right.



### 5.3: Testing for dominance/recessiveness of suppressor strains

Spontaneous and UV-derived *bud23Δ* growth phenotype suppressor mutants were mated to AJY2682 and diploids were selected on Nat/G418 plates. As a homozygous diploid *bud23Δ* growth control AJY2682 was also mated to AJY2676 and selected on the same media. Diploids were then compared with the control *bud23Δ* diploid strain for growth rate. If a particular suppressor mutant is recessive then I would expect the suppressor-containing diploid strain to grow at the same rate as the homozygous diploid *bud23Δ* control. If a particular suppressor mutant is dominant, then I would expect the suppressor containing diploid strain to grow better than the homozygous diploid *bud23Δ* control. When the strains were compared it revealed that all of the mutants isolated appeared to be dominant.

### 5.3: Testing for aneuploidy in *bud23Δ* suppressor strains

It is possible that the mutants that suppress the *bud23Δ* growth phenotype are instances of aneuploidy that increase the dosage of a gene that enables the strain bearing the extra chromosome to grow better. Three pieces of data point to aneuploidy as a possible explanation. First over-expression of *RPS2*, present on chromosome VII, allows *bud23Δ* strains to grow better so there may be an extra chromosome VII present in AJY2684. Second an analysis of strain collections indicated a high incidence of aneuploidy among strains bearing a deletion of one paralog of ribosomal proteins that are present as pairs of paralogs [53]. It is possible that a similar situation may exist for ribosome biogenesis factors. Even though ribosome biogenesis factors do not exist as

paralogs, more copies of a particular factor may provide a selective advantage when *BUD23* is deleted. Third, and related to the second, the fact that we see these suppressors arise relatively often indicates that there is a relatively large mutagenic target space, such as the ribosomal proteins or biogenesis factors. In order to rule out aneuploidy of chromosome VII specifically, and other chromosomes in general, two approaches were taken to detect aneuploidy. The first is Southern-blot based, and the second uses a genetic test.

In approach one, Southern blotting was carried out on DNA from WT, AJY2676 (*bud23Δ*), and AJY2683 (suppressor), using probes for *NMD3* (chromosome VIII) and *RPS2* (chromosome VII). These blots were then quantitated for band intensity for both the *NMD3* band and the *RPS2* band. If ratio of the *NMD3*:*RPS2* band intensities is identical between WT, *bud23Δ*, and suppressor mutant strains, this would indicate that there are the same number of *RPS2* and *NMD3* loci, and thus no aneuploidy. This is what was observed (Figure 5.3). The *NMD3*:*RPS2* band intensity ratios were identical in each strain when images were analyzed using ImageJ [43].

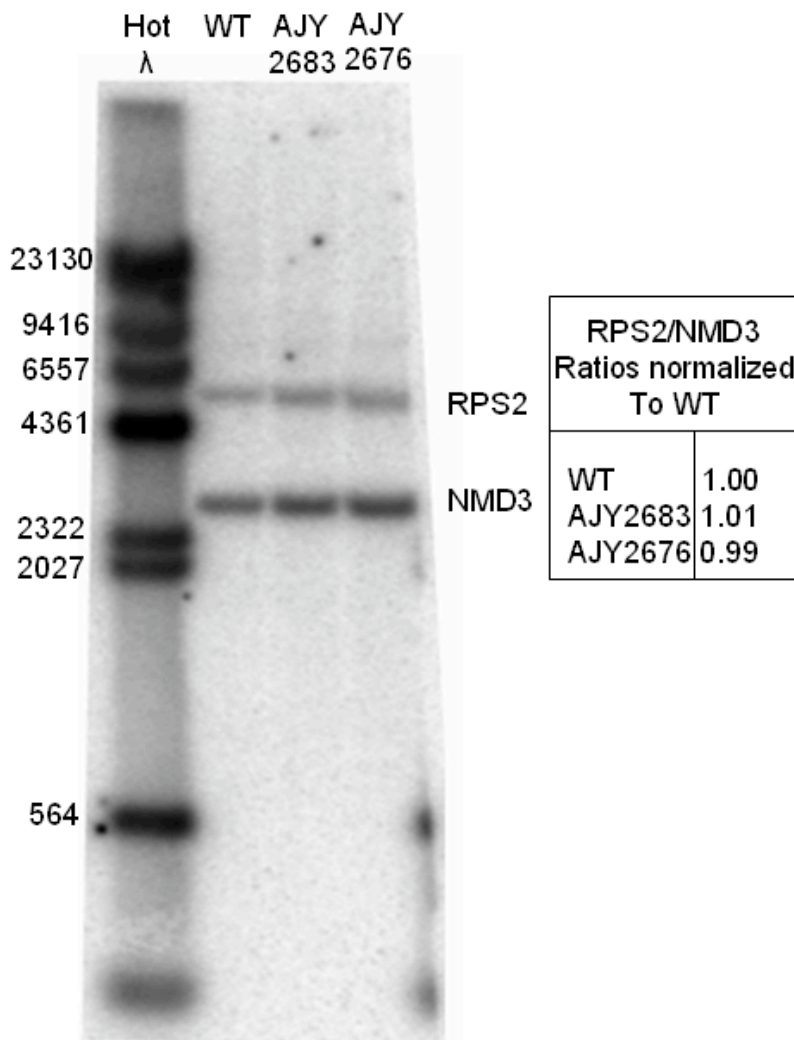


**Figure 5.3: Southern blot demonstrating that the ratios of *RPS2* signal to *NMD3* signal are the same in WT, *bud23Δ*, and suppressor mutants.**

DNA was extracted from WT, AJY2676 (*bud23Δ*), and *bud23Δ* suppressor mutant (AJY2683) and analyzed for amount of *RPS2* and *NMD3* DNA using southern blotting. The ratios of *RPS2/NMD3* are identical in all strains indicating that multicopy *RPS2* is not a likely explanation for the suppression of the *bud23Δ* phenotype suppression. Band intensity ratio values were normalized to the WT ratio.

While we could be certain that there was the same *NMD3* and *RPS2* ratio in the spontaneous suppressor strain and the wild-type, we could not be sure there was no aneuploidy for another chromosome. Instead of testing each chromosome against each other individually we decided that it would be simpler to use a genetic test (Illustrations 5.1 and 5.2). The genetic approach to detecting aneuploidy takes advantage of the fact that recombination is suppressed for genes that are closely linked to centromeres, in this case *TRP1*. If the growth suppression is due to aneuploidy, sporulating a diploid that is homozygous for *bud23Δ*, and heterozygous for both *trp1Δ*, and *bud23Δ* growth suppressor phenotype should yield no tetratypes (see Illustrations 4 and 5 for explanation). If the suppression is due to a mutation, tetratypes should be observed. When this screen was carried out 12 viable tetrads were obtained that yielded 6 tetratypes, indicating that the suppressor mutant is not due to aneuploidy and is in fact a bonafide dominant mutant.

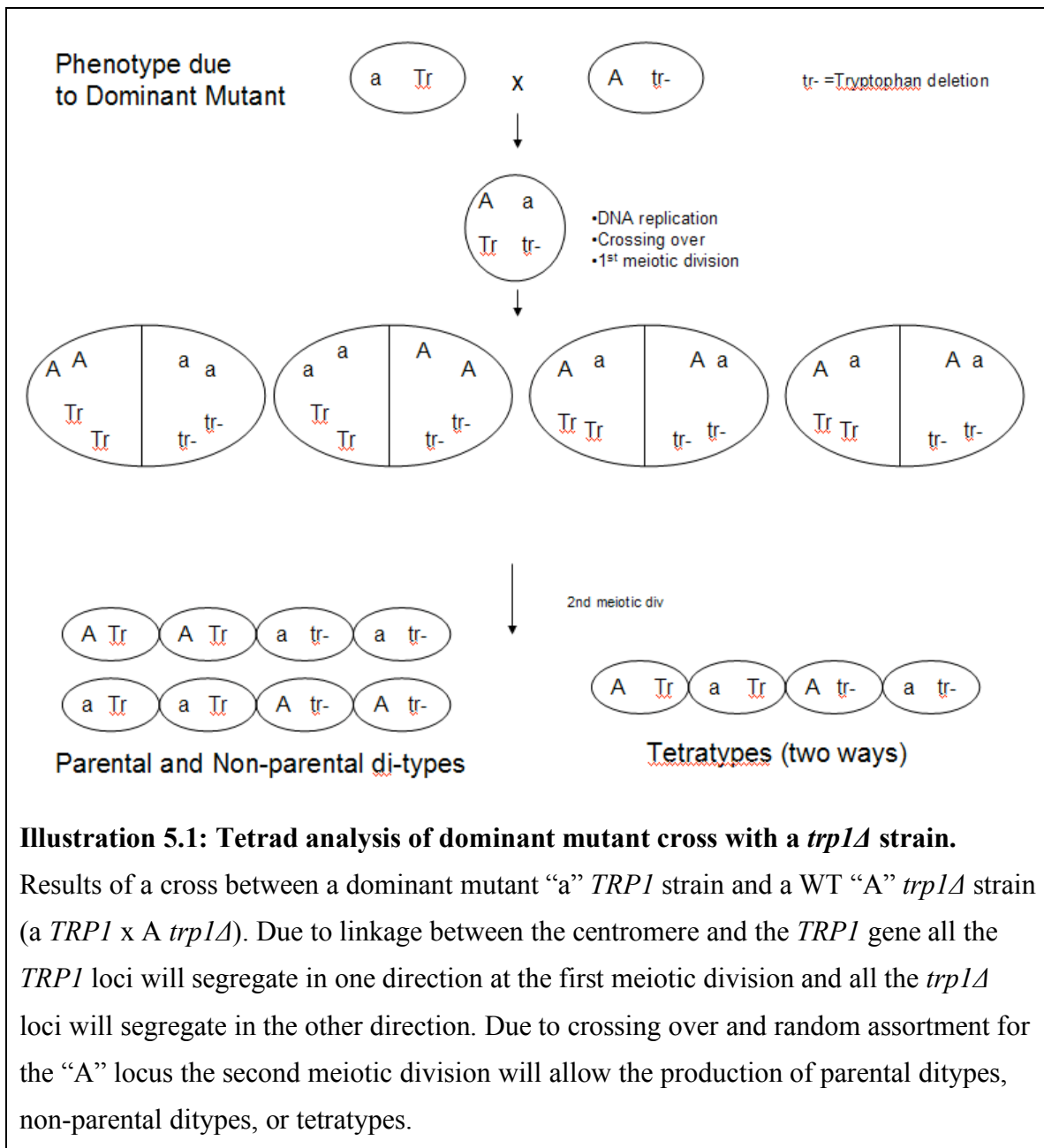


**Illustration 5.1: Tetrad analysis of dominant mutant cross with a *trp1Δ* strain.**

Results of a cross between a dominant mutant “a” *TRP1* strain and a WT “A” *trp1Δ* strain ( $a \text{ } \underline{TRP1}$  x  $A \text{ } \underline{trp1Δ}$ ). Due to linkage between the centromere and the *TRP1* gene all the *TRP1* loci will segregate in one direction at the first meiotic division and all the *trp1Δ* loci will segregate in the other direction. Due to crossing over and random assortment for the “A” locus the second meiotic division will allow the production of parental di-types, non-parental di-types, or tetratypes.

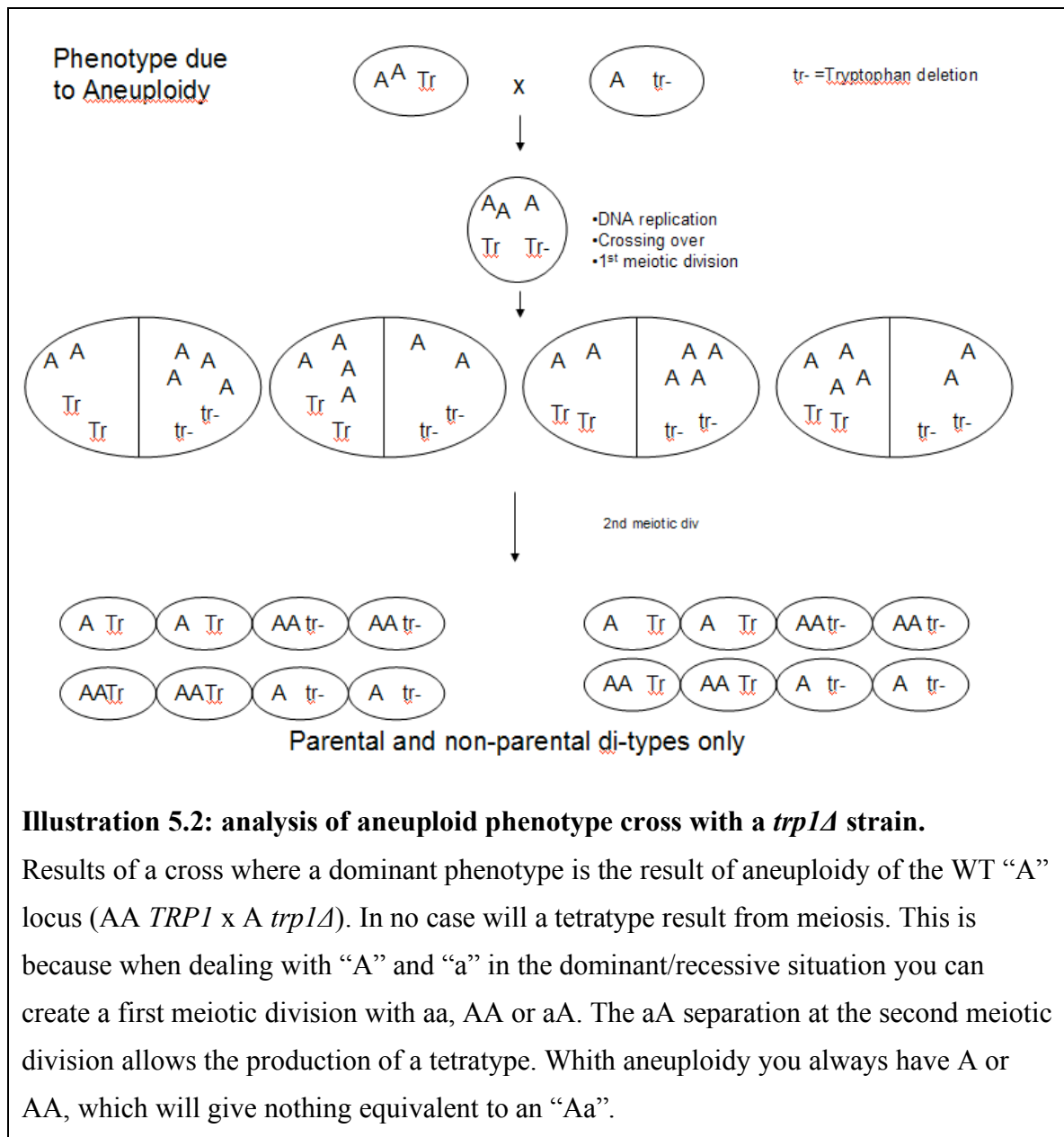


**Illustration 5.2: analysis of aneuploid phenotype cross with a *trp1Δ* strain.**

Results of a cross where a dominant phenotype is the result of aneuploidy of the WT “A” locus ( $AA \text{ TRP1}$  x  $A \text{ trp1}\Delta$ ). In no case will a tetatype result from meiosis. This is because when dealing with “A” and “a” in the dominant/recessive situation you can create a first meiotic division with aa, AA or aA. The aA separation at the second meiotic division allows the production of a tetatype. With aneuploidy you always have A or AA, which will give nothing equivalent to an “Aa”.

#### **5.4: *bud23Δ* suppressor comparison with multicopy *RPS2* expression**

As mentioned previously *RPS2* was isolated as a multicopy suppressor of the *bud23Δ* growth phenotype. We were interested in how the growth of the suppressor strain AJY2683 compared to the growth of a *bud23Δ* strain expressing multicopy Rps2. A *bud23Δ* strain (AJY2676) was transformed with multicopy *RPS2* (pAJ1652), *BUD23* (pAJ1654) and empty vector (pRS426). AJY2683 grew significantly better than the *bud23Δ* strain expressing multicopy *RPS2* demonstrating that suppressor mutant is better at recovering growth than multicopy *RPS2* (Figure 5.4). Neither suppressor grew as well as the strain expressing multicopy *BUD23*.

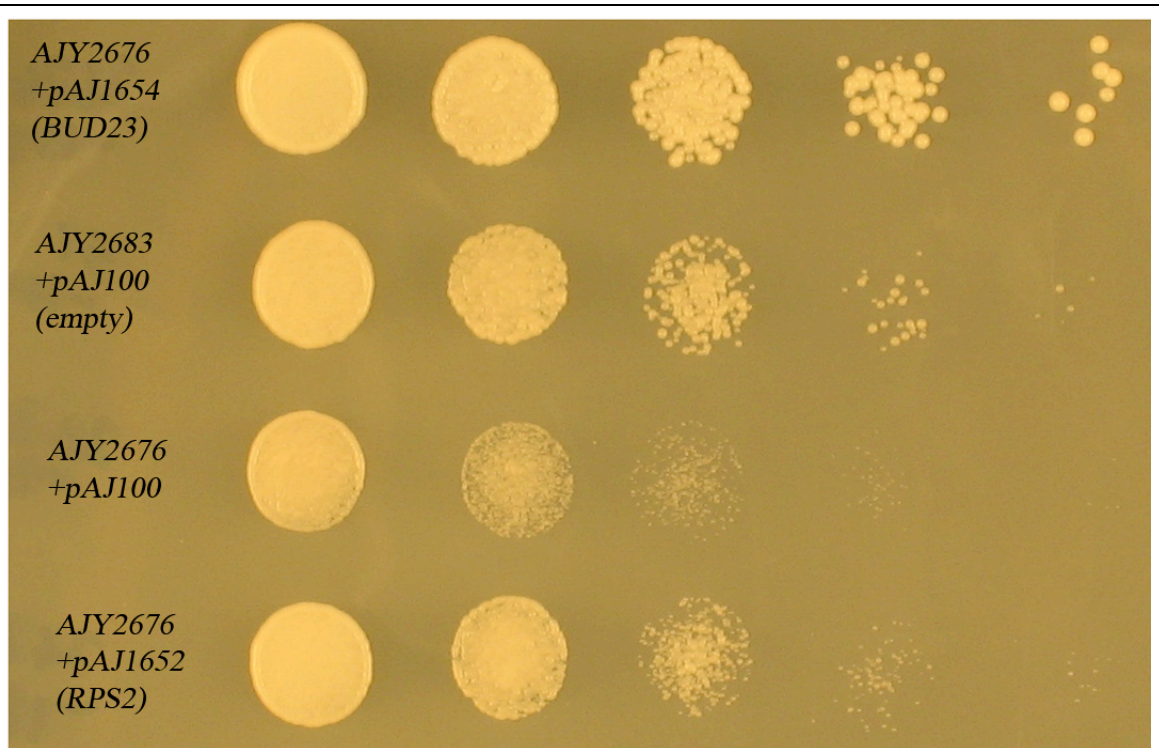


**Figure 5.4: Comparison between *bud23Δ* suppressor AJY2683 and *RPS2* multicopy suppression of the *BUD23* deletion phenotype.**

*BUD23* deletion strain AJY2676 was transformed with either empty vector (pAJ100), WT *BUD23* (pAJ1654), or multicopy *RPS2* (pAJ1652). The suppressor mutant is better able to suppress the *BUD23* deletion growth phenotype than over expression of *RPS2*.

### 5.5: Analysis of polysome profiles of *bud23Δ* suppressor mutant containing strains.

Strains in which *BUD23* has been deleted have polysomal profiles that indicate a defect in the production of 40S ribosomal subunits (Figure 1). Since the suppressor mutants grow better than their parental *bud23Δ* strain, we wanted to see if there was any evidence in the polysome profiles for how this suppression relieves the *bud23Δ* growth defect. Four strains were compared; WT (AJY1942), *bud23Δ* (AJY2676), suppressor in a *bud23Δ* background (AJY2684), and suppressor in a WT *BUD23* background (AJY2688) (Figure 5.5). Comparisons between WT and *bud23Δ* were the same as previously described [12], (dark blue= WT, magenta= *bud23Δ*). When *bud23Δ* strain is compared to the double mutant AJY2683 (*bud23Δ* + suppressor, yellow), features indicative of a recovery of 40S are observed. This comparison displays a drop in the level of 60S, an increase in the level of 80S, and a small recovery of polysomes. No obvious increase in the level of 40S is observed, however the 40S is not visible in both profiles for both AJY2676 (*bud23Δ*) and AJY2683 (double mutant) (Figure 5.5). When the suppressor single mutant is compared to the WT strain there is no significant difference at any point along the profile.

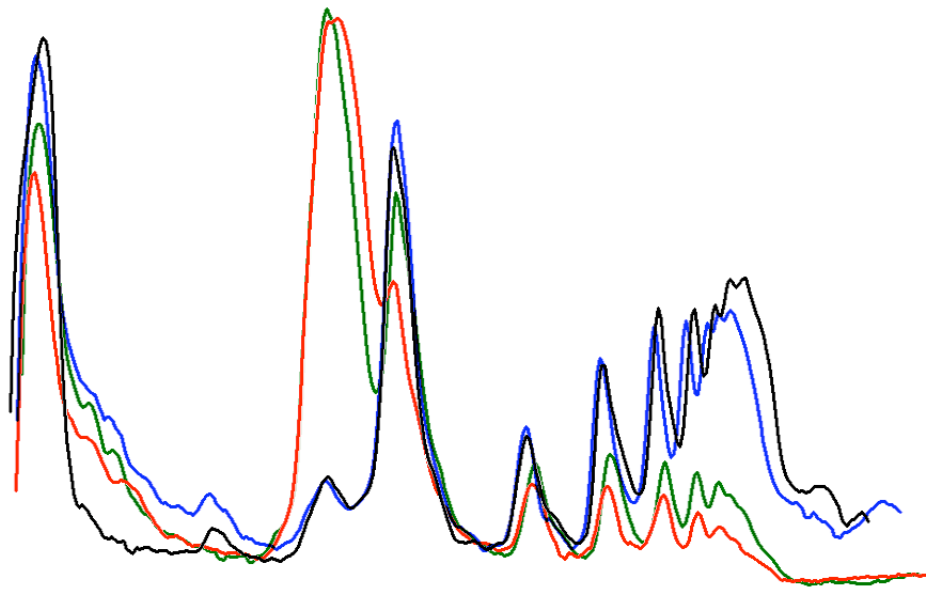


**Figure 5.5: Polysomal profiles of WT, *bud23Δ*, suppressed *bud23Δ*, and isolated suppressor mutation indicate that suppression may be due to increased production of 40S subunits.**

Liquid cultures of WT (black), *bud23Δ* (red), suppressed *bud23Δ* (green), and isolated suppressor mutant AJY2688 (WT *BUD23*) (blue) were grown and harvested in the presence of cyclohexamide. Protein was extracted, separated on sucrose gradients, and fractionated while measuring absorbance at A<sub>260</sub>. Comparison between *bud23Δ* (magenta) and suppressed *bud23Δ* (yellow) reveals a decrease in the level of 60S and an increase in the level of polysomes.

## 5.6: Identification of *UTP14* as the *bud23Δ* suppressor

In order to identify the mutant gene that was improving the *bud23Δ* growth phenotype a Sau3AI partial digested genomic library was constructed from the spontaneous suppressor strain AJY2683. The library was transformed into AJY2676. Three hundred candidate colonies that grew faster than AJY2676 were chosen and most of these candidates were eliminated as not plasmid dependant or not restoring suppressor growth rate. One isolate showed the appropriate plasmid dependent growth rate. The plasmid contained in that colony was purified and sequenced and its insert contained only one intact gene, *UTP14* (Illustration 5.3). Sequencing the *utp14* clone revealed a single mutation; a C to G mutation at position 2273 resulting in an amino acid change of alanine to glycine at position 578. Interestingly when the mutant *UTP14* was transformed into the *bud23* deletion strain AJY2676, the suppression was not as great (Figure 5.6) suggesting that the mutant does not compete efficiently with the endogenous wild-type Utp14. Now named pAJ1918, the *UTP14*(A758G) vector was cut with SnaBI and BstEI which removed all of the 5' end of UTP14 and all but ~180 base pairs of the 3' end. This gapped vector was then transformed into AJY1942 and colonies that repaired the vector by recombination with WT *UTP14* were selected on URA<sup>-</sup> plates. This WT *UTP14* vector was named pAJ1919. Sequencing with AJO1293 confirmed that the A758G mutation was not present. Expression of WT *UTP14* from pAJ1919 in AJY2676 did not suppress the *bud23Δ* growth defect indicating that suppression was solely due to the *UTP14*(A758G) gain-of-function mutation (data not shown).

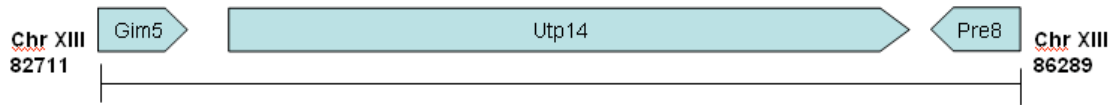
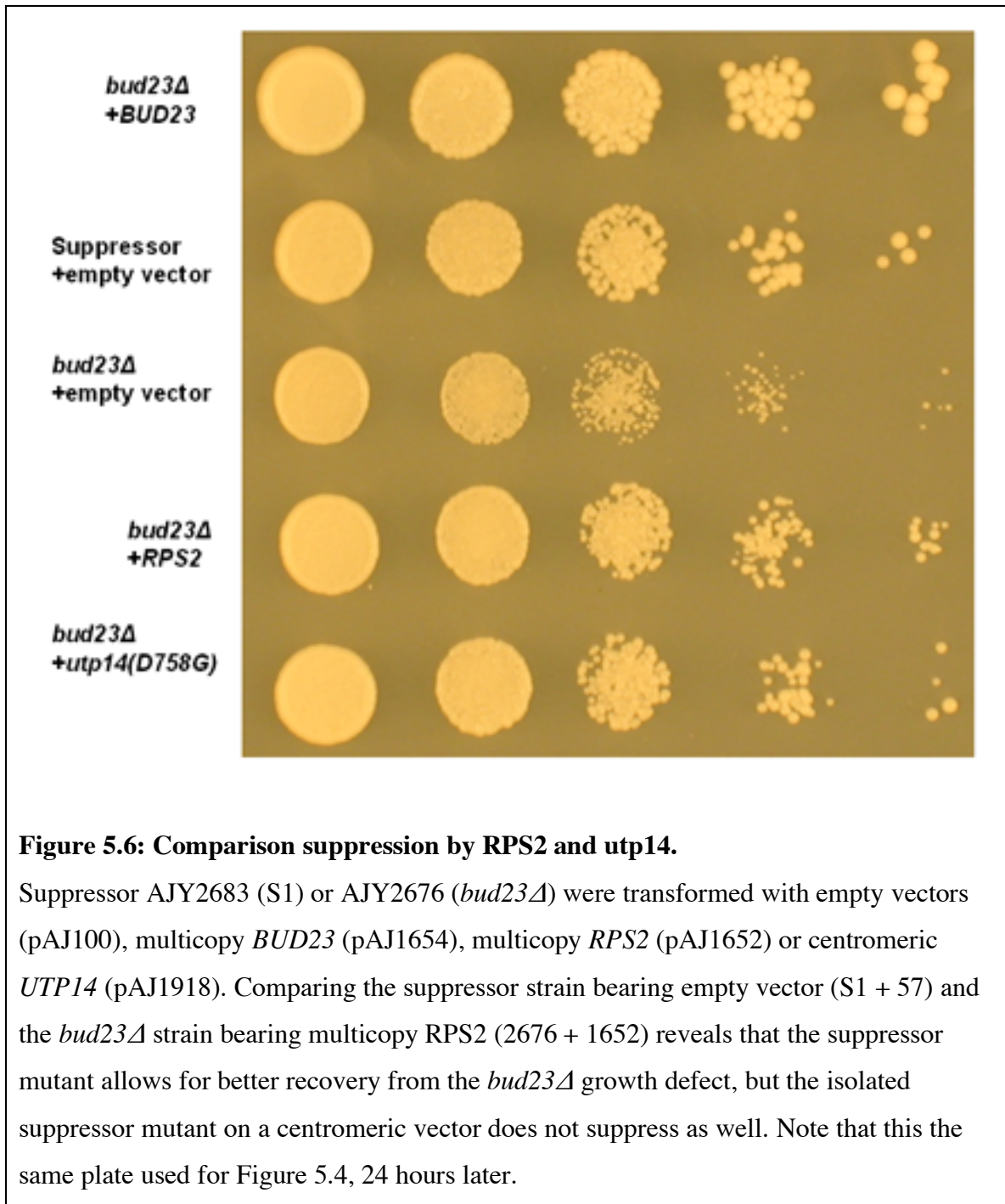


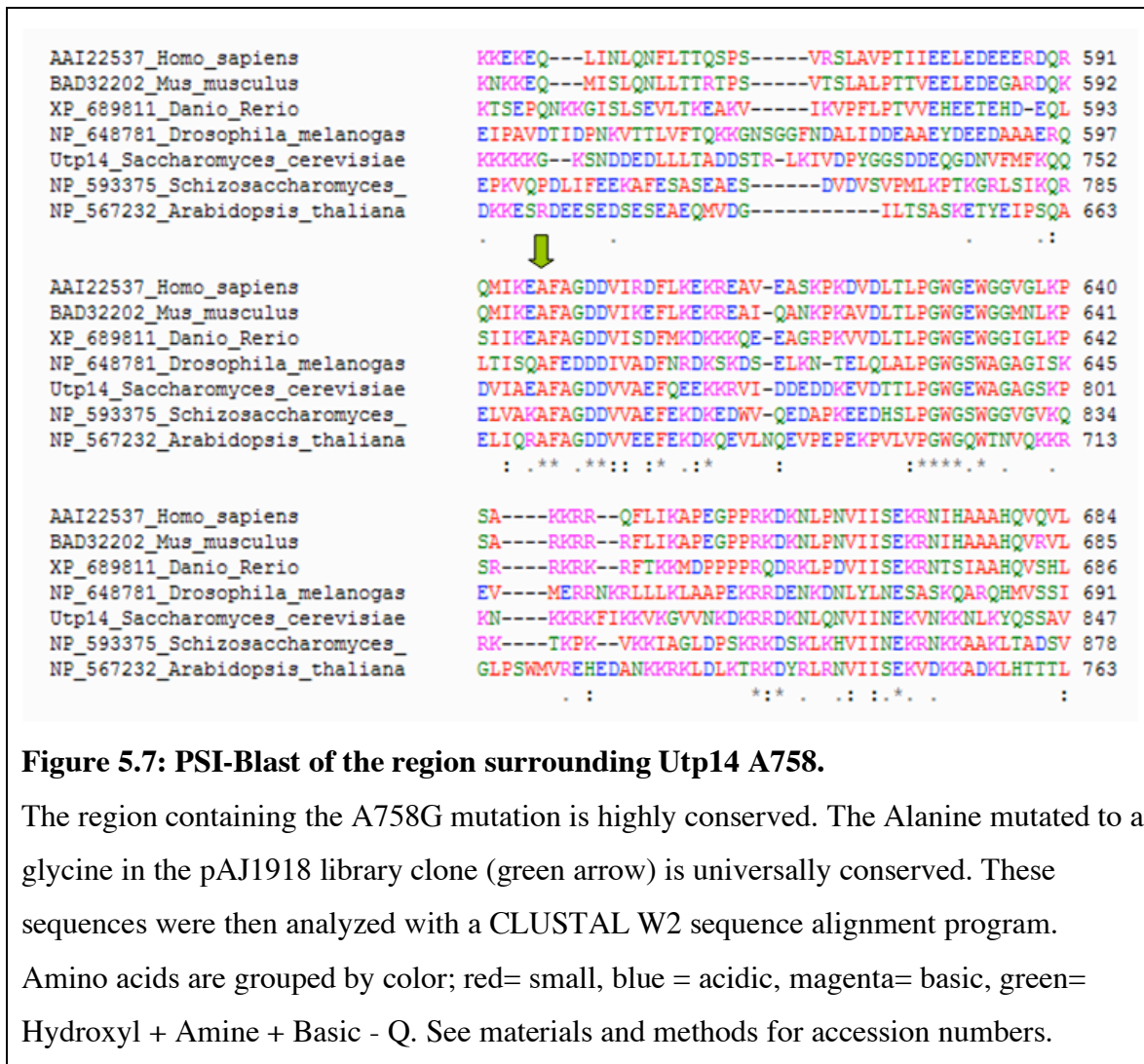
**Illustration 5.3: Diagram of the insert identified from the AJY2683 genomic library.**

*bud23Δ* suppressor strain AJY2693 genomic DNA was partially digested and inserted into pRS416 to create a genomic library. The resulting library was transformed into AJY2676 and faster growing colonies were screened for dominant suppression of *BUD23* deletion phenotype. The above insert was found in the clone that suppressed the *bud23Δ* growth phenotype. Note that only 138 base pairs of *GIM5* (out of 489) and 450 base pairs of *PRE8* (out of 750) were present in this library clone.



## **5.7 Sequence comparison of Utp14**

Utp14 is a nucleolar localized 899 amino acid protein that is part of the small subunit processome [5]. Utp14 is essential and depletion of Utp14 results in elimination of all cleavage events that lead to 20S formation (A0, A1, A2) indicating that it is involved in the production of small subunits. A protein BLAST search was carried out at the National Center for Biotechnology Information website in order to identify homologs of Utp14. All results returned were eukaryotic proteins and no search within archaea or eubacteria returned sequences with significant similarity. A PSI-BLAST search using a selection of the protein blast results revealed that the majority of the C-terminus including the region around A758 is highly conserved, and the alanine itself seems to be universally conserved within Utp14 homologs (Figure 5.7).

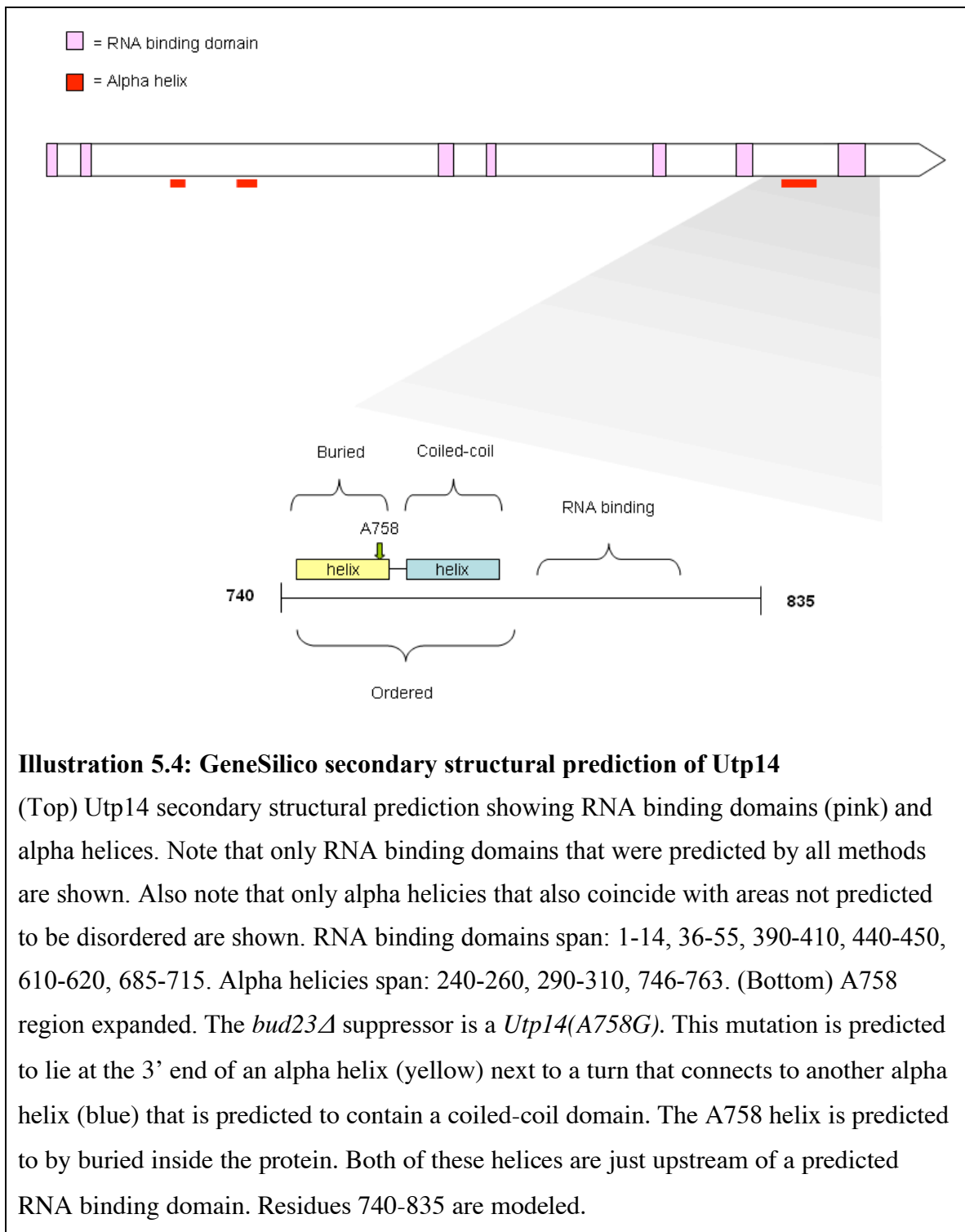


## **5.8 Secondary structure prediction of the region surrounding A758.**

The amino acid sequence for Utp14 was analyzed using the GeneSilico metaserver [45]. Two sequences were analyzed: all 899 amino acids, and the last 500 amino acids. The reason for this is because more accurate analysis is possible with smaller sequences, and the analysis of the shorter sequence resulted in the detail of the A758 region in Illustration 5.4. Because there are no structures for Utp14 or related proteins, this analysis is restricted to secondary structure predictions (Illustration 5.4). In general Utp14 is an 899 amino acid protein that contains several predicted RNA binding domains and a few alpha helices. It is likely that there are more alpha helices present in Utp14, but the helices in Illustration 5.4 were the only ones to pass the criteria I set. Only alpha helices that also correspond with regions predicted to not be disordered were included. In order to add as much certainty as possible to these predictions for RNA binding domains, I only included regions of at least ten residues predicted by all three methods. It should be noted that for a protein involved in rRNA processing, Utp14 has a pI of ~5 indicating that it is not basic overall [44].

All relevant predicted structural information was included in a more detailed illustration of the region in which the mutation lies. The consensus of 13 modeling methods showed that A758 lies in the center of a region not predicted to be disordered spanning residues N745-E767 (Illustration 5.4). Approximately 30 residues downstream from A758 is a potential RNA binding region of ~30 base pairs. Another consensus of 9 methods puts A758 on the 5' end of a 15 amino acid alpha helix (V746-A760), two amino acids on the 5' side of a turn (G761-D763) connecting to another 15 amino acid

alpha helix (V764-D778). Several residues within the disordered region are predicted to be buried including A758. Finally, the last significant secondary structural prediction is a putative coiled-coil domain spanning V765-E779 in the putative alpha-helix downstream of the helix containing A758. Coiled-coil domains are known to be involved in protein-protein interactions [54].



## **Discussion**

### **The general nature of suppressors of the *bud23Δ* growth defect**

*BUD23* deletion strains are able to acquire suppressor mutations that display a range of growth recovery (Figure 5.1) that at best surpasses the ability of *RPS2* over expression to recover growth. Analysis of polysomes from the AJY2683 suppressor reveals that one likely explanation for the increased growth rate is an increased level of 40S available to join with 60S. This is shown by the small decrease in the level of free 60S and the small increase in the level of polysomes. A similar result was seen in a polysomal analysis of *RPS2* over expression (personal communication Richa Sardana). A possible explanation for the growth recovery was aneuploidy resulting in the over expression of a gene (such as *RPS2*) that would result in increased 40S production. However two approaches for the detection of aneuploidy failed to detect any aneuploidy. The best conclusion is that AJY2683 suppresses the *bud23Δ* growth defect at the locus of interaction as a result of a dominant mutant that has the effect of increasing the production of mature 40S subunits.

### ***Utp14(A758G)* is a dominant suppressor of the *bud23Δ* growth phenotype.**

When a genomic library was made from AJY2683, a clone was isolated that produced suppression in AJY2676, but to a lesser extent than the suppression in AJY2683. This is probably because the suppressor now has to compete with the wild-type version of the gene. Sequencing that clone revealed a C to G mutation at position

2273 in *utp14* that results in an alanine to glycine missense mutation. Utp14 (U Three associated Protein) is a nucleolar localized, essential protein that is part of the small subunit processome, a protein complex that functionally and physically overlaps with the 90S particle and is visualized as the small terminal knobs in Miller spreads [3-5, 55]. This complex is thought to guide the folding of the pre-40S and direct the A0-A2 cleavage events that trim the 35S rRNA and liberate the 20S rRNA as a pre-40S particle. Precisely where Utp14 fits into early ribosome biogenesis is difficult to determine since it has not appeared in many purifications of 90S/SSU processome complexes. Grandi et al. isolated what is thought to be the earliest 90S particles using TAP tagged proteins [6]. These purifications did not yield Utp14. It was not until Dragon et al. used a similar approach that purified specifically U3 associated proteins that Utp14 was discovered [5]. However a latter attempt using different SSU processome proteins did not find Utp14 [56]. Most recently Utp14 appeared in a validation experiment for an RNP purification methodology by Oeffinger et al. using Utp2 (Nop14) [57]. Given these data it is impossible to position Utp14 in the 40S assembly pathway since it could be a factor only needed for a brief biogenesis step, or some of the purification conditions used may not have been favorable for isolation of Utp14 along with the rest of the complex.

Depletion of Utp14 results in a loss of all SSU processing species (18S, 20S, 21S, 22S) and an accumulation of the unusual 23S processing intermediate that results from cleavage at site A3 when cleavage is absent at sites A0-A2 [5, 55]. Interestingly, the work that established the detailed depletion phenotype also showed a modest decrease in the level of 35S when Utp14 is depleted [55]. While Gallagher et al. did not specifically

mention Utp14 as causing a 35S depletion phenotype, a significant difference is seen when reexamining the data they present. A potential role for Utp14 in the transcription of the 35S is further supported by other recent work analyzing proteins that complex with the transcription factor Mot1 [58]. Mot1 is an unusual transcription factor that is known to both repress and enhance transcription [59, 60] and one target of its enhancement role is the transcription of 35S rRNA [60]. Work by Arnett et al. showed that Mot1 interacts with a wide range of transcriptional co-regulators [58]. Utp14 was identified in this work as a protein that interacts with Mot1.

### **Connections between Utp14, Bud23 and explanation of *bud23Δ* suppression**

What is the nature of the suppression of the *bud23Δ* growth defect? Because Utp14 is a nucleolar protein, the nucleolar defect of *bud23Δ* strains is likely to be the event that is suppressed. Bud23-GFP has a nuclear localization with a nucleolar focus [12] and westerns of polysome profile fractions show Bud23-GFP present in a region that would correspond to the 90S (Richa Sardana, personal communication). Utp14 plays its only known role in the nucleolus and likely binds before Bud23 since depletion of Utp14 prevents all cleavages that normally produce a normal 20S, including the 5' cleavages [55]. Schafer et al. detected Bud23 in whole cell extract and pre-40S, but not 90S where it was likely present, but under-represented relative to other 90S sized particles [7]. Close inspection of Figure 4.5 shows that *BUD23* deletion seems to have an effect on both the nuclear and the nucleolar localization of ITS1. When the nucleolar ITS1 signals of the WT, LMB+, LMB-, and *bud23Δ* strains are compared, similar levels of nucleolar ITS1 are seen between WT, LMB+, and LMB- suggesting that these cells carry out nucleolar

events at similar rates. However when *BUD23* is deleted the levels of nucleolar ITS1 increase dramatically suggesting that the rRNA containing ITS1 accumulates in the nucleolus. When analyzing the nucleoplasmic ITS1 levels, these levels appear similar when comparing WT/LMB- or *bud23Δ*/LMB+ strains. This suggests that blocking nuclear export only causes nuclear accumulation of ITS1 and deletion of *BUD23* leads to nuclear *and* nucleolar accumulation of ITS1. With respect to Utp14, the mutant would likely improve the nucleolar maturation events, but not the nuclear events.

How is this suppression occurring? This depends on the nucleolar role of Bud23 and Utp14. It is likely that Bud23 promotes nucleolar maturation, or Bud23 prevents inhibition of maturation. Possibilities include: release of factors, binding of factors, or folding of rRNA. Examples of the first possibility, release of factors, are found in large subunit biogenesis factors. In the large subunit release of Tif6 is aided by the non-essential GTPase, Efl1[61]. When *EFL1* was deleted the localization of Tif6 shifts to the cytoplasm and the strain grows more slowly. A dominant suppressor in Tif6 was obtained that restored growth and nuclear localization [61]. It is possible that binding of Bud23 is linked to release of Utp14, or release of another factor through Utp14. If this is the case *utp14(A758G)* may be released more readily in the absence of Bud23. Bud23 has no known homology to proteins such as GTPases or helicases that act in the removal of protein factors and RNAs. Since it is a methyltransferase with highly conserved positively charged regions it likely plays a structural role consistent with “structural proofreading”. As the pre-40S matures it eventually reaches a state of maturation that allows binding of Bud23. In the absence of Bud23, the pre-40S may be locked into a

conformation where the function of Utp14 is inhibited. If release of Utp14 or another factor is altered in the suppressor, this may bypass a GTPase or helicase whose function is no longer necessary in the *utp14A758G* strain.

Fluorescent in situ hybridization should be performed to determine the affect of *utp14(A758G)* on the nucleolar and nuclear ITS1 localization. If the hypothesis presented above is correct and *utp14(A758G)* is partially abrogating the need for Bud23 in the nucleolus, then a reduced nucleolar ITS1 intensity may be visible in both cases. If no ITS1 decrease or even an increase is observed the *utp14(A758G)* may be allowing as much or more pre-40S to be produced, but a later nucleolar block remains. Both cases would provide clues about the 40S biogenesis pathway.

### **Export defects of Utp14 and Bud23.**

It is unlikely that the Utp14 mutation identified here has any effect on nucleoplasmic events. If the *utp14(A758G)* is able to restore nucleolar events to nearly normal processing and export then further work with Bud23 in a *utp14(A758G)* background may make it easier to study its role in export to the cytoplasm by eliminating nucleolar phenotypes. But it should be noted that it is still possible that a cytoplasmic export factor may need Bud23 for normal nucleolar binding. The Utp14 mutation may yet affect such a factor and affect cytoplasmic export.

### **A model for Bud23, Utp14 and 40S biogenesis.**

See Illustration 5.5. Utp14 likely binds very early in biogenesis and binds before Bud23. When Bud23 binds it stabilizes the 90S/pre-40S in a manner that promotes the normal function of Utp14 and binding of Rps2. When Rps2 is successfully bound the pre-40S then exits the nucleolus when sufficiently mature. There may be a functional link between Rps2 binding and Bud23 related function of Utp14. After nucleolar exit the pre-40S must then become competent for export to the cytoplasm. This process likely involves the binding of more protein factors such as export adaptors and may involve further rRNA rearrangements. Both protein binding and rRNA folding may require Bud23 either for direct recruitment of a protein, or the creation of a proper binding site.

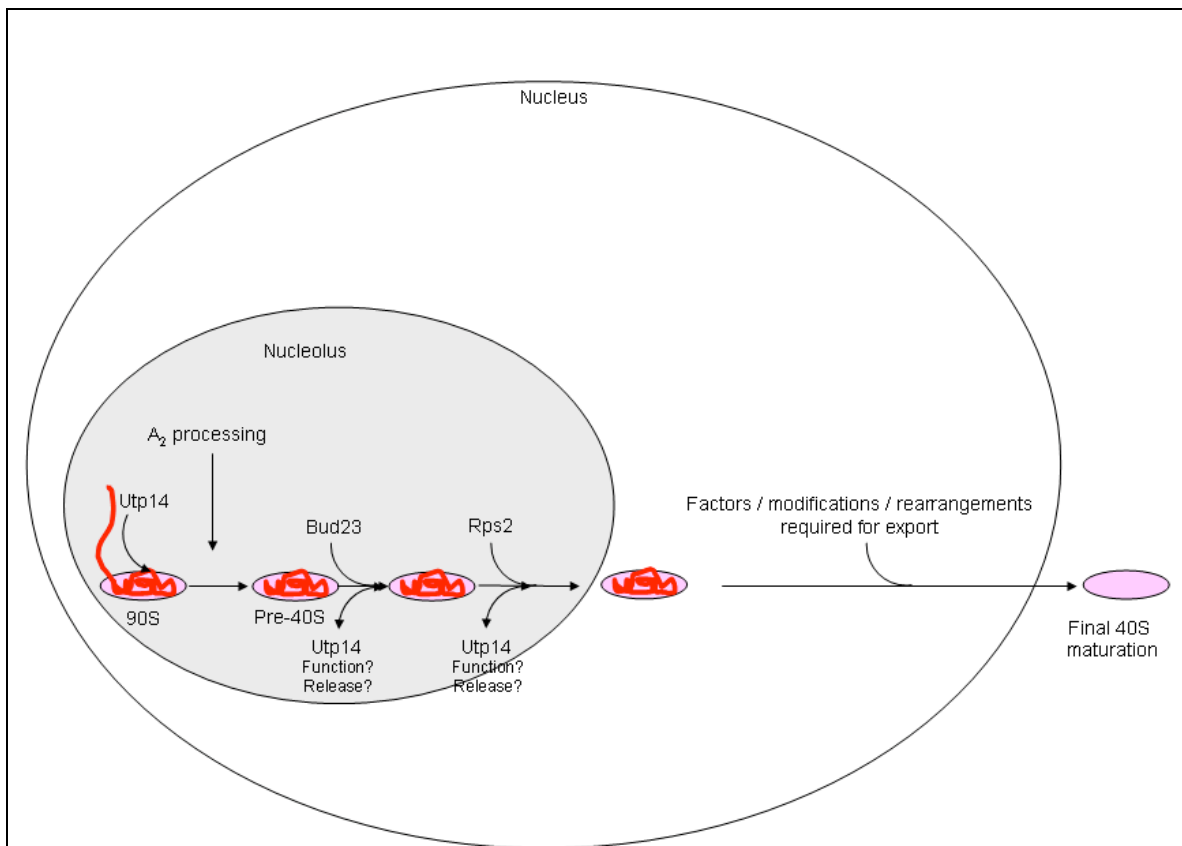


**Illustration 5.5: Model for the role of Utp14 and Bud23 in 40S biogenesis.**

Utp14 binds first and is required for A0-A2 processing. Bud23 binds after Utp14 and is required for changes that allow for pre-40S export from the nucleolus including proper binding of Rps2. After nucleolar export Bud23 is also required for the normal nucleoplasmic events that lead to export possibly including export factors or rRNA remodeling. In the absence of Bud23 the nucleolar consequence may be that function/release of Utp14 is less efficient, and Rps2 loading may be directly or indirectly delayed by lack of Bud23 or presence of Utp14. Nucleoplasmic consequences of lack of Bud23 involve problems with maturation steps import to export. Such problems should still be present in the suppressor strain.

## Bibliography

1. Li, Z., et al., *Rational Extension of the Ribosome Biogenesis Pathway Using Network-Guided Genetics*.
2. Planta, R.J., *Regulation of ribosome synthesis in yeast*. Yeast, 1997. **13**(16): p. 1505-18.
3. Henras, A.K., et al., *The post-transcriptional steps of eukaryotic ribosome biogenesis*. Cell Mol Life Sci, 2008. **65**(15): p. 2334-59.
4. Fromont-Racine, M., et al., *Ribosome assembly in eukaryotes*. Gene, 2003. **313**: p. 17-42.
5. Dragon, F., et al., *A large nucleolar U3 ribonucleoprotein required for 18S ribosomal RNA biogenesis*. Nature, 2002. **417**(6892): p. 967-70.
6. Grandi, P., et al., *90S pre-ribosomes include the 35S pre-rRNA, the U3 snoRNP, and 40S subunit processing factors but predominantly lack 60S synthesis factors*. Mol Cell, 2002. **10**(1): p. 105-15.
7. Schafer, T., et al., *The path from nucleolar 90S to cytoplasmic 40S pre-ribosomes*. Embo J, 2003. **22**(6): p. 1370-80.
8. Mougey, E.B., et al., *The terminal balls characteristic of eukaryotic rRNA transcription units in chromatin spreads are rRNA processing complexes*. Genes Dev, 1993. **7**(8): p. 1609-19.
9. Moy, T.I. and P.A. Silver, *Nuclear export of the small ribosomal subunit requires the ran-GTPase cycle and certain nucleoporins*. Genes Dev, 1999. **13**(16): p. 2118-33.
10. Fatica, A., D. Tollervy, and M. Dlakic, *PIN domain of Nob1p is required for D-site cleavage in 20S pre-rRNA*. Rna, 2004. **10**(11): p. 1698-701.
11. Combs, D.J., et al., *Prp43p is a DEAH-box spliceosome disassembly factor essential for ribosome biogenesis*. Mol Cell Biol, 2006. **26**(2): p. 523-34.
12. White, J., et al., *Bud23 methylates G1575 of 18S rRNA and is required for efficient nuclear export of pre-40S subunits*. Mol Cell Biol, 2008. **28**(10): p. 3151-61.
13. Seiser, R.M., et al., *Ltv1 is required for efficient nuclear export of the ribosomal small subunit in Saccharomyces cerevisiae*. Genetics, 2006. **174**(2): p. 679-91.

14. Fatica, A., et al., *Nob1p is required for cleavage of the 3' end of 18S rRNA*. Mol Cell Biol, 2003. **23**(5): p. 1798-807.
15. Nierhaus, K.H., *The assembly of prokaryotic ribosomes*. Biochimie, 1991. **73**(6): p. 739-55.
16. Held, W.A., et al., *Assembly mapping of 30 S ribosomal proteins from Escherichia coli. Further studies*. J Biol Chem, 1974. **249**(10): p. 3103-11.
17. Ferreira-Cerca, S., et al., *Analysis of the in vivo assembly pathway of eukaryotic 40S ribosomal proteins*. Mol Cell, 2007. **28**(3): p. 446-57.
18. Dez, C., J. Houseley, and D. Tollervey, *Surveillance of nuclear-restricted pre-ribosomes within a subnucleolar region of Saccharomyces cerevisiae*. Embo J, 2006. **25**(7): p. 1534-46.
19. Lafontaine, D.L., T. Preiss, and D. Tollervey, *Yeast 18S rRNA dimethylase Dim1p: a quality control mechanism in ribosome synthesis?* Mol Cell Biol, 1998. **18**(4): p. 2360-70.
20. Schafer, T., et al., *Hrr25-dependent phosphorylation state regulates organization of the pre-40S subunit*. Nature, 2006. **441**(7093): p. 651-5.
21. Gerton, J.L., et al., *Inaugural article: global mapping of meiotic recombination hotspots and coldspots in the yeast Saccharomyces cerevisiae*. Proc Natl Acad Sci U S A, 2000. **97**(21): p. 11383-90.
22. Johnson, A.W., E. Lund, and J. Dahlberg, *Nuclear export of ribosomal subunits*. Trends Biochem Sci, 2002. **27**(11): p. 580-5.
23. Decatur, W.A. and M.J. Fournier, *rRNA modifications and ribosome function*. Trends Biochem Sci, 2002. **27**(7): p. 344-51.
24. Bachellerie, J.P., J. Cavaille, and A. Huttenhofer, *The expanding snoRNA world*. Biochimie, 2002. **84**(8): p. 775-90.
25. Esguerra, J., J. Warringer, and A. Blomberg, *Functional importance of individual rRNA 2'-O-ribose methylations revealed by high-resolution phenotyping*. Rna, 2008. **14**(4): p. 649-56.
26. Khaitovich, P., et al., *Reconstitution of functionally active Thermus aquaticus large ribosomal subunits with in vitro-transcribed rRNA*. Biochemistry, 1999. **38**(6): p. 1780-8.
27. King, T.H., et al., *Ribosome structure and activity are altered in cells lacking snoRNPs that form pseudouridines in the peptidyl transferase center*. Mol Cell, 2003. **11**(2): p. 425-35.
28. Xu, Z., et al., *A conserved rRNA methyltransferase regulates ribosome biogenesis*. Nat Struct Mol Biol, 2008. **15**(5): p. 534-6.

29. Lafontaine, D., et al., *The DIM1 gene responsible for the conserved m6(2)Am6(2)A dimethylation in the 3'-terminal loop of 18 S rRNA is essential in yeast*. J Mol Biol, 1994. **241**(3): p. 492-7.
30. Leulliot, N., et al., *The yeast ribosome synthesis factor Emg1 is a novel member of the superfamily of alpha/beta knot fold methyltransferases*. Nucleic Acids Res, 2008. **36**(2): p. 629-39.
31. Liang, X.H., Q. Liu, and M.J. Fournier, *rRNA modifications in an intersubunit bridge of the ribosome strongly affect both ribosome biogenesis and activity*. Mol Cell, 2007. **28**(6): p. 965-77.
32. Liang, X.H., Q. Liu, and M.J. Fournier, *Loss of rRNA modifications in the decoding center of the ribosome impairs translation and strongly delays pre-rRNA processing*. Rna, 2009.
33. Liu, B., et al., *Mis-targeted methylation in rRNA can severely impair ribosome synthesis and activity*. RNA Biol, 2008. **5**(4): p. 249-54.
34. Ni, L. and M. Snyder, *A genomic study of the bipolar bud site selection pattern in Saccharomyces cerevisiae*. Mol Biol Cell, 2001. **12**(7): p. 2147-70.
35. Piekna-Przybylska, D., W.A. Decatur, and M.J. Fournier, *The 3D rRNA modification maps database: with interactive tools for ribosome analysis*. Nucleic Acids Res, 2008. **36**(Database issue): p. D178-83.
36. Kaiser C, M.S., Mitchell A, *Methods in yeast genetics*. 1994: Cold Spring Harbor Laboratory Press.
37. Winzeler, E.A., et al., *Functional characterization of the S. cerevisiae genome by gene deletion and parallel analysis*. Science, 1999. **285**(5429): p. 901-6.
38. Wintermeyer, W. and H.G. Zachau, *A specific chemical chain scission of tRNA at 7-methylguanosine*. FEBS Lett, 1970. **11**(3): p. 160-164.
39. Boyle A, P.-O.K., *Current protocols in molecular biology*. 1992, New York, NY: John Wiley and Sons.
40. Altschul, S.F., et al., *Basic local alignment search tool*. J Mol Biol, 1990. **215**(3): p. 403-10.
41. Larkin, M.A., et al., *Clustal W and Clustal X version 2.0*. Bioinformatics, 2007. **23**(21): p. 2947-8.
42. Sambrook, J. and D.W. Russell, *Random Priming: Radiolabeling of Purified DNA Fragments by Extension of Random Oligonucleotides*. Cold Spring Harbor Protocols, 2006. **2006**(2): p. pdb.prot3542-.

43. Abràmoff M. D., M.P.J., Ram S. J. , *Image Processing with ImageJ*. Biophotonics International, 2004. **11**(7): p. 36-42.
44. Chervitz, S.A., et al., *Using the Saccharomyces Genome Database (SGD) for analysis of protein similarities and structure*. Nucleic Acids Res, 1999. **27**(1): p. 74-8.
45. Kurowski, M.A. and J.M. Bujnicki, *GeneSilico protein structure prediction meta-server*. Nucleic Acids Res, 2003. **31**(13): p. 3305-7.
46. Vanrobays, E., et al., *Dim2p, a KH-domain protein required for small ribosomal subunit synthesis*. Rna, 2004. **10**(4): p. 645-56.
47. Chen, W., et al., *Enp1, a yeast protein associated with U3 and U14 snoRNAs, is required for pre-rRNA processing and 40S subunit synthesis*. Nucleic Acids Res, 2003. **31**(2): p. 690-9.
48. Niewmierzycka, A. and S. Clarke, *S-Adenosylmethionine-dependent methylation in Saccharomyces cerevisiae. Identification of a novel protein arginine methyltransferase*. J Biol Chem, 1999. **274**(2): p. 814-24.
49. Moy, T.I. and P.A. Silver, *Requirements for the nuclear export of the small ribosomal subunit*. J Cell Sci, 2002. **115**(Pt 14): p. 2985-95.
50. Oeffinger, M., M. Dlakic, and D. Tollervey, *A pre-ribosome-associated HEAT-repeat protein is required for export of both ribosomal subunits*. Genes Dev, 2004. **18**(2): p. 196-209.
51. Tijerina, P., S. Mohr, and R. Russell, *DMS footprinting of structured RNAs and RNA-protein complexes*. Nat Protoc, 2007. **2**(10): p. 2608-23.
52. Perreault, A., C. Bellemer, and F. Bachand, *Nuclear export competence of pre-40S subunits in fission yeast requires the ribosomal protein Rps2*. Nucleic Acids Res, 2008. **36**(19): p. 6132-42.
53. Hughes, T.R., et al., *Widespread aneuploidy revealed by DNA microarray expression profiling*. Nat Genet, 2000. **25**(3): p. 333-7.
54. Burkhard, P., J. Stetefeld, and S.V. Strelkov, *Coiled coils: a highly versatile protein folding motif*. Trends Cell Biol, 2001. **11**(2): p. 82-8.
55. Gallagher, J.E., et al., *RNA polymerase I transcription and pre-rRNA processing are linked by specific SSU processome components*. Genes Dev, 2004. **18**(20): p. 2506-17.
56. Bernstein, K.A., et al., *The small-subunit processome is a ribosome assembly intermediate*. Eukaryot Cell, 2004. **3**(6): p. 1619-26.

57. Oeffinger, M., et al., *Comprehensive analysis of diverse ribonucleoprotein complexes*. Nat Methods, 2007. **4**(11): p. 951-6.
58. Arnett, D.R., et al., *A proteomics analysis of yeast Mot1p protein-protein associations: insights into mechanism*. Mol Cell Proteomics, 2008. **7**(11): p. 2090-106.
59. Dasgupta, A., et al., *Mot1 activates and represses transcription by direct, ATPase-dependent mechanisms*. Proc Natl Acad Sci U S A, 2002. **99**(5): p. 2666-71.
60. Dasgupta, A., et al., *Regulation of rRNA synthesis by TATA-binding protein-associated factor Mot1*. Mol Cell Biol, 2007. **27**(8): p. 2886-96.
61. Senger, B., et al., *The nucle(ol)ar Tif6p and Efl1p are required for a late cytoplasmic step of ribosome synthesis*. Mol Cell, 2001. **8**(6): p. 1363-73.

## **Vita**

Joshua Paul White was born in Tucson, Arizona on February 24 1977 to Michael Fredrick White and Christine Sue Thomas. He earned a bachelors degree in Cell and Molecular Biology from the University of Arizona in 2002, and a bachelors degree in Microbiology from the University of Arizona in 2003. After two years as a technician he then joined the graduate program at the University of Texas at Austin in 2005, studying in the laboratory of Dr. Arlen Johnson.

Permanent address: 1207 Southport Dr. Appt #105, Austin, TX, 78704

This thesis was typed by the author